Construction and Building Materials 201 (2019) 852–870

Contents lists available at ScienceDirect

Construction and Building Materials

journal homepage: www.elsevier.com/locate/conbuildmat

Nanolime- and nanosilica-based consolidants applied on heated granite and limestone: Effectiveness and durability

J.S. Pozo-Antonio [a,*], J. Otero [b], P. Alonso [c], X. Mas i Barberà [c]

[a] Depto. de Enxeñaría de Recursos Naturais e Medioambiente, Universidade de Vigo, 36310 Vigo, Spain
[b] The J. Paul Getty Trust, Getty Conservation Institute, Los Angeles, CA CA90049, USA
[c] Instituto Universitario de Restauración del Patrimonio, Ciutat Politècnica de la Innovació, Universitat Politècnica de València, 46022 Valencia, Spain

HIGHLIGHTS

- Both granite and limestone increased the porosity after the heating process.
- Granite: Nanorestore and NanoEstel yielded similar reduction of porosity and resistance to salt cycles.
- Limestone: Nanorestore® yielded lower effectiveness due lower penetration.
- NanoEstel® yielded higher decay after salt cycles in the limestone due to lower compatibility.

ARTICLE INFO

Article history:
Received 13 October 2018
Received in revised form 20 December 2018
Accepted 31 December 2018
Available online 11 January 2019

Keywords:
Stone
Nano-silica
Nano-lime
Granite
Limestone

ABSTRACT

This paper shows a study on the consolidation effectiveness of nano-silica and nano-lime-based consolidants (i.e. Nano Estel®and Nanorestore®, respectively), both available on the market, on two stones with different mineralogy and texture (i.e. two micas granite and Lioz limestone) previously subjected to 500 °C during 24 h with a rapid cooling by water jet simulating the real practice in a fire. The consolidation effectiveness was determined through the evaluation of hydro-physical properties (i.e. open porosity, apparent density, water absorption by capillarity and water absorption at atmospheric pressure), the determination of P-wave velocity (compressional wave velocity) and the study of their side-effects by using stereomicroscopy, colour spectrophotometry, Fourier transform infrared spectroscopy and scanning electron microscopy. Durability of the consolidants was determined by measuring their resistance to salt crystallization cycles and the subsequent surfaces were evaluated by open porosity measurements, stereomicroscopy, Fourier transform infrared spectroscopy and scanning electron microscopy. Results showed, as expected, that both granite and limestone samples increased their porosity after the heating process. In the case of granite stone, both products yielded similar reduction of the porosity and similar resistance to salt crystallization cycles. In case of limestone, nanolime samples yielded lower effectiveness in terms of dry matter, porosity, and water absorption by capillary coefficient, which is attributed to the low penetration of Nanorestore® particles in the fine pore structure of this stone. Ethyl silicate treated samples presented higher levels of decay after crystallization cycles in the limestone samples, which could be attributed to the difficulty to bond silicate materials to fine porous calcite-based substrates.

1. Introduction

Consolidation of deteriorated stones is a common intervention to strengthen the stone surfaces and to mitigate the disintegration process. Treatment is applied to substrates with lack of superficial cohesion due to different alteration processes. Deterioration processes (e.g. crystallization of soluble salts, fires, abrasion, among others) induce serious deterioration patterns such as stone granular disintegration or sanding and scaling on the stones surfaces which seriously jeopardize the preservation of architectural heritage [1]. Regarding deterioration processes, fire (natural or arson related) induces physical–chemical changes and mechanical damages caused by the heat, followed by the shock cooling by water jet applied to extinguish the fire. As result, fissures density and fissures length increase and the stone can suffer losses of material [2–5]. Fires reaching temperatures higher than 800 °C have a significant effect on the stone's physical–chemical and mechanical properties and the developed effects, mainly spalling, are not recoverable [6]. However, in areas which were subjected to lower

* Corresponding author.
E-mail address: ipozo@uvigo.es (J.S. Pozo-Antonio).

https://doi.org/10.1016/j.conbuildmat.2018.12.213
0950-0618/

temperature gradient (~500 °C), among the main deterioration patterns related to porosity changes and neoformed minerals, are scaling, flaking and granular disaggregation [1,5,7,8].

Granite and limestone are very important construction materials in buildings and monuments worldwide. Granite is a polymineralic stone composed mainly by quartz, feldspar, plagioclase and biotite, while limestone is composed mainly of calcite [9]. Calcite based materials present higher susceptibility than granite due to the dissolution of calcite mineral when water, CO_2 and pollutants are involved [9–11]. However, both stones can be severely affected by high temperature due to fires inducing changes of physical–mechanical properties. Therefore, in order to preserve stones that were affected by fires, since their mechanical properties are not remarkably affected and then spalling did not occur, the application of consolidants to enhance the superficial cohesion seems to be a suitable alternative. Since consolidation is an irreversible intervention, the correct choice of the consolidant is very important. Therefore, it is recommended to perform some tests to determine the suitability of the consolidant.

Since 1960s, synthetic organic materials such as acrylic, epoxy or vinyl resins have been continuously used to consolidate several historic stones. However, several drawbacks were reported due to changes of stone porosity, capillarity, permeability to water vapour and wettability [12,13]. Moreover, a yellowing of the consolidated surfaces was also observed [14]. Therefore, in order to avoid these problems, inorganic consolidants, such as ethyl silicate, calcium hydroxide (limewater), barium hydroxide, calcium oxalate and calcium tartrate were mostly considered, being the first two the most commonly used ones. Ethyl silicate-based consolidants are mainly composed by alkosylanes; they polymerise *in situ* inside the pore, through a classic sol–gel process [15,16]. Alkoxysilane groups in contact with ambient moisture, hydrolysed producing silanol groups releasing ethanol, which evaporates. After a polymerization process these silanol groups are transformed into siloxanes, releasing water [17,18]. The low viscosity of alkoxysilane allows the penetration into the stone through fissures and the formation of siloxane bonds [17,18]. This low viscosity prevents the dilution in organic solvents. However, these products during the polymerization started to show fissures and fractures since the evaporation of the solvent causes a concave interface of the liquid into the pores of the gel due to the different surficial tensions [19,20]. As result, the gel with some rigidity cannot endure the contraction and the consolidate layer fractures.

On the other hand, the other commonly used inorganic consolidant is the limewater. In this technique, after carbonation, the calcium hydroxide ($Ca(OH)_2$) induces a network of calcite ($CaCO_3$) consolidating materials which are highly compatible with the calcite matrix [13,21]. However, as it was reported by the silica-based consolidant, the $Ca(OH)_2$ based consolidant showed also some significant drawbacks being the most important the low solubility of $Ca(OH)_2$ particles in water (1.7 $g.L^{-1}$ at 20 °C, [22]). This leads that an application of limewater requires a large amount of aqueous solutions to achieve consolidating effects and therefore, large amounts of water can favour the pore collapse through freeze–thaw cycles, the transport of soluble salts and the biological colonization [23]. Brajer and Kalsbeek already reported in 1999 that to achieve a positive consolidation, limewater should be uninterruptedly applied over 80 days [22]. Moreover, low penetration of the product and the subsequent veiling of the surfaces due to the fast carbonation of the $Ca(OH)_2$ aqueous dispersions were also reported [24,25].

Then, in order to minimize the cited drawbacks and negative effects of the consolidants, i.e. the formation of fractures in case of the ethyl silicate-based consolidants and the use of large amount of water and poor penetration with the limewater, nano-particles started to become very popular to enhance the dispersion stability, the penetration through fissures and, in case of calcium hydroxide, the reactivity of the particles to CO_2 [13,23,26–31]. In the case of nanolime, the use of alcohol as a carrier of lime nanoparticles allows carrying higher amount of particles, yields deeper penetration with less water and induces a faster carbonation [13,31,32]. Nanolimes have emerged as an efficient consolidant for the superficial consolidation of different historic substrates (e.g. wall-paintings, stuccos or plasters) [30], stones [33,34] and for the conservation of other cultural heritage materials such as paper [35], canvas [36], bones [37] and wood [38]. Nanolimes preserve the same compatibility of the traditional limewater treatment while presenting superior consolidation properties. The main advantages are: i) nanolimes contain higher amounts of calcium hydroxide particles; ii) nanoparticles are more reactive due to their higher specific surface thus carbonation occurs faster; iii) nanolimes obtain higher penetration depths due to the smaller particle size [13,31].

Regarding to the application of nanosilica-based consolidants on stone, Nano Estel®, which was used throughout this study, has been applied on ignimbrites from the complex of Tokali in Göreme and the Church of the Forty Martyrs at Şahinefendi (Turkey) [39]. It showed worse penetration and cohesion than the solvent-based products of ethyl silicate Estel 1000® and Estel 1100® [39]. However, Estel 1100® contains organic groups, that under outdoor exposition, could induce oxidation processes. Therefore, it is considered that it should be limited to indoor environments. Moreover, Nano Estel® did not alter the porous network of the stone. The water suspension of nanosilica Syton X30® applied on a pyroclastic stone increased the resistance to salt crystallization although the Estel 1000® dispersed in organic solvent showed a better behaviour in terms of superficial cohesion [40].

Regarding to nanolime-based products on stones, several authors reported the insufficient penetration of the nanolime [13,31]. Nanorestore® and Calosil® and their migration to the surface in limestone and lime-mortars highlight the relevance of the pore structure and nanolime properties (such as the type of solvent and particle size) on the consolidation effectiveness [27,41–44]. In a recent study [45], based on a suitability study of the ultrasonic tomography technique to evaluate the distribution of consolidants (the ethyl silicate Tegovakon® and the dispersion of nanolime particles Nanorestore®) throughout the Lioz limestone (previously subjected to 600 °C), concluded that Nanorestore® did not achieve a significant reduction of the open porosity suggesting that the consolidation achieved was not as satisfactory as for the Tegovakon® consolidated samples. Despite Zornoza-Indart et al. [46] reported an increase in the drying kinetics of natural stone after the application of nano-lime, Musacchi and Diaz Gonçalvez [25] did not find any increase of the drying kinetics after the application of nano-treatments (nanolime- and also nanosilica-based consolidants) on both limestone and sandstone.

Other study compared two nano-particle consolidants with different composition (nanolime Calosil E25® and nanosilica Nano Estel®) applied on two different kind of stones: Ançã limestone and Bentheimer sandstone, both with open porosity higher than 17% [25]. It was concluded that both products did not affect the kinetics of drying process, without changing the drying rate. However, from the aesthetical point of view, the nanolime gave a whitish tone to the surfaces and the nanosilica gave them a significant shine tone noticeable to the naked eye.

In this paper, the effectiveness of two nanoconsolidants with different compositions (nanosilica and nano-calcium hydroxide particles) available on the market was evaluated on two stones with different mineralogy and texture, a granite and a limestone, commonly found in the Spanish and Portuguese cultural heritage, respectively. Previously to the consolidant application, samples were subjected to 500 °C during 24 h and cooled down to room temperature using tap water jet. After nanoconsolidants

application, the effectiveness and also the durability of both products in terms of the resistance to salt crystallization cycles were evaluated.

2. Materials and methods

2.1. Stones

Two different stones belonging to the cultural heritage of Iberian Peninsula were selected. A granite ashlar was obtained from the ancient asylum *Hermanitas de los Ancianos Desamparados* located in Vigo's old quarter (NW Spain). It is a two-mica granite associated with the Hercynian orogeny [47] commonly used as building stone in the historic centres of Vigo and Pontevedra (NW Spain). It is a fine grained equigranular granite (2–0.3 mm), composed of quartz (29%), potassium feldspar (25%), sodium plagioclase (24%), muscovite (13%) and biotite (4%) as main minerals [48]. Average open porosity (accessibility to water following [49]) was 4.41%.The pore size distribution was obtained by Mercury Intrusion Porosimetry (MIP) using a Micromeritics Autopore IV9500 porosimeterthat works with two pressure ranges, 0.20 MPa–225 MPa (high pressure) and 14 kPa–0.20 MPa (low pressure). The pore network charge (zeta potential) was determined using a Zetasizer Nano Z, from Malvern Instruments. The test was carried out on one fragment collected from the surface of a 4 cm × 4 cm × 4 cm-cube measuring approximately 2 cm × 2 cm × 2 cm. MIP shows that the granite stone has some coarser pores with diameters between 50 μm and 100 μm, intermediate pores with diameters between 1 μm and 50 μm and finer pores with diameters between 0.06 μm and 1 μm (Fig. 1A).

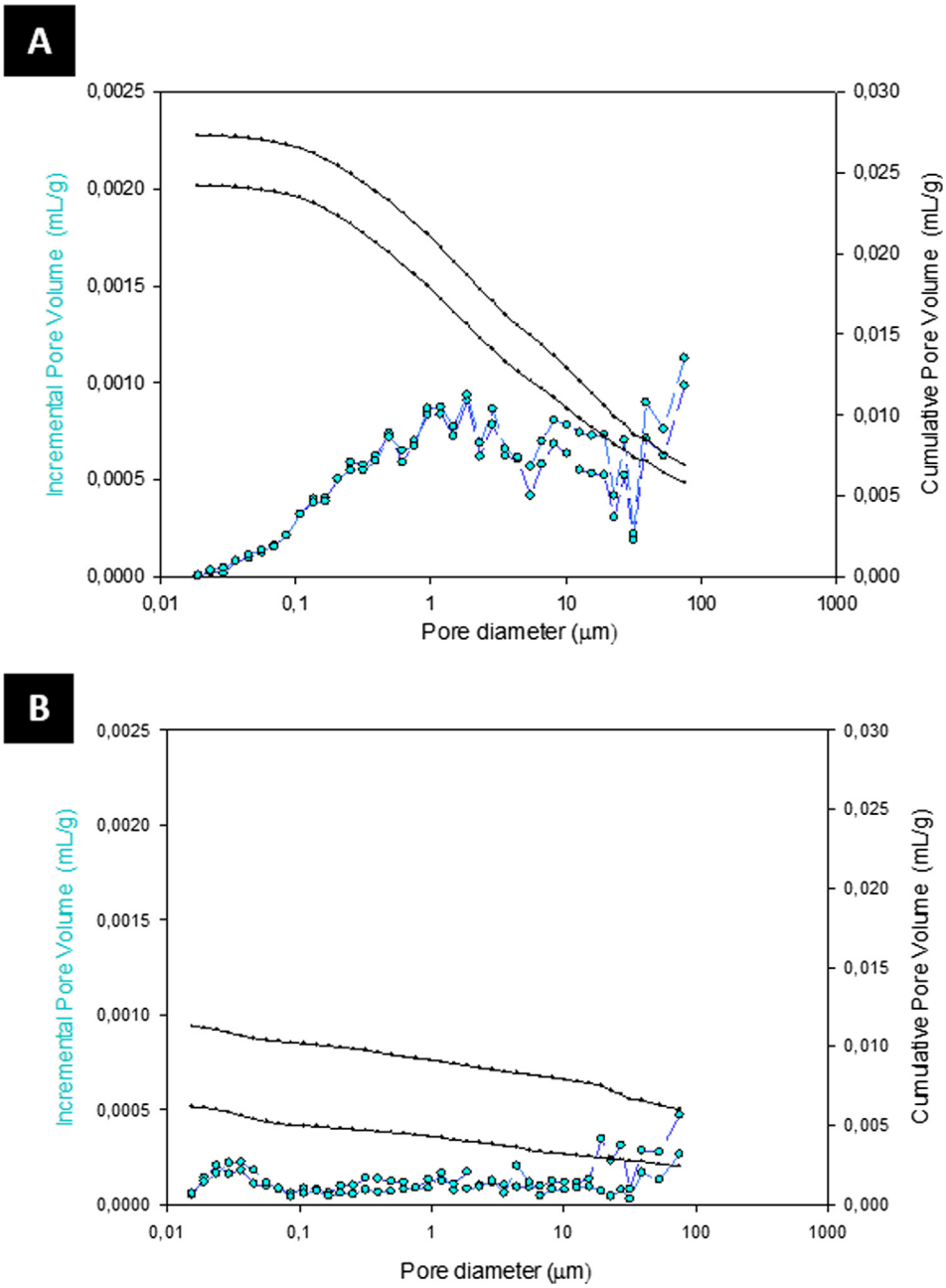

Fig. 1. Differential volume of intruded mercury versus pore diameter of: A) granite stone; B) Lioz limestone.

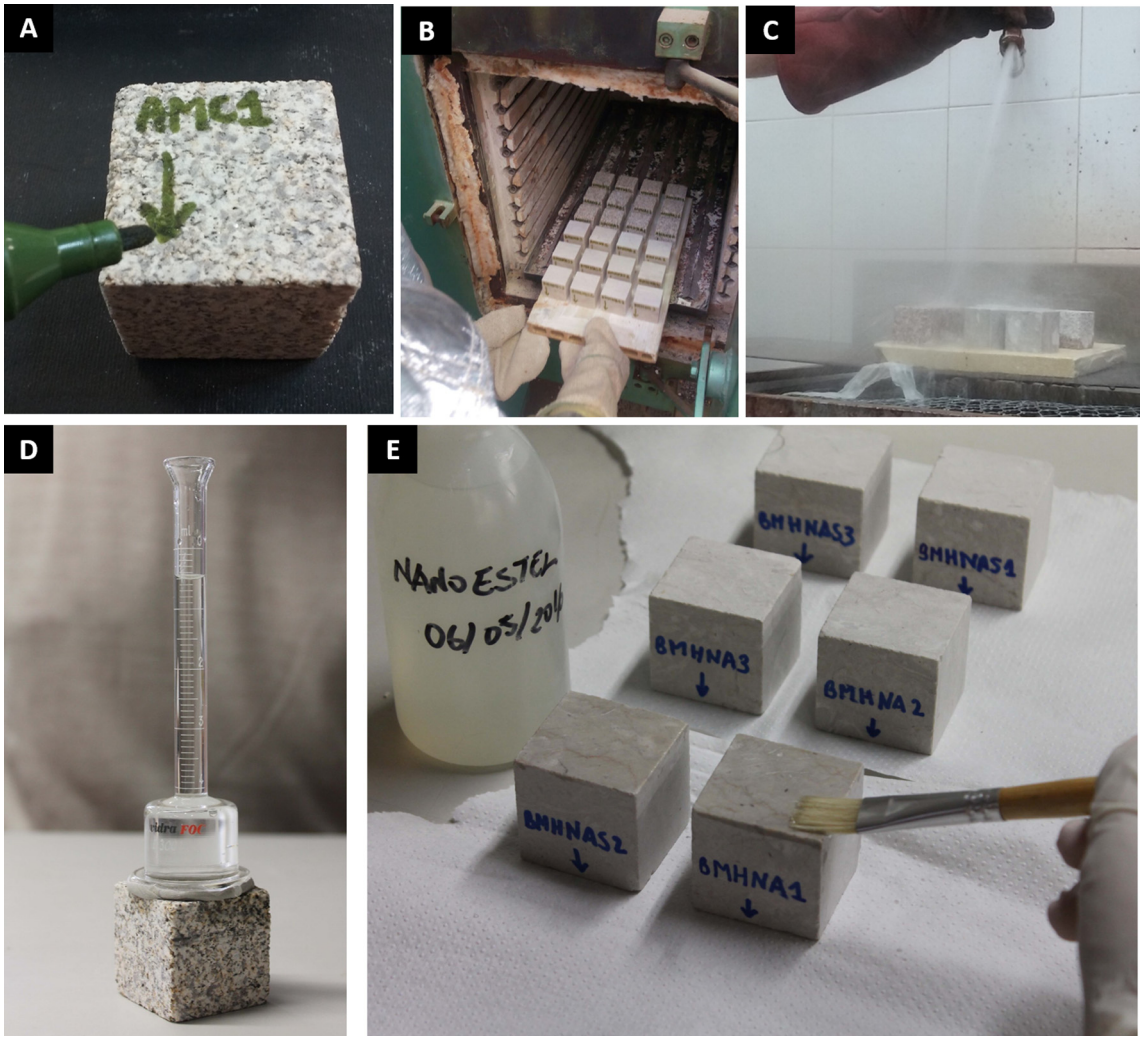

Fig. 2. Digital photographs of the samples and methodology used in the preparation of the samples. A: 4 cm × 4 cm × 4 cm – granite cubes. B: samples after 500 °C in an industrial oven. C: samples being subjected to a shock cooling by tap water jet. D: application of Karsten pipe method following [54]. E: application of NE on the limestone samples. NE: Nano Estel.

As a limestone, the Cretacic Lioz limestone used in Lisbon's old quarter (Portugal centre) was selected. It is a coarse cream microcrystalline bioclastic and calciclastic limestone [50]. It is characterized by the presence of stylolites. This stone presents a very low value of open porosity (average water accessible porosity following [49]) was 0.3%. MIP shows that the Lioz limestone has a fine pore structure, presenting pores with diameters between 0.02 and 0.08 μm and between 0.08 and 20 μm; and some coarse pores between 20 μm and 100 μm (Fig. 1B). For each stone, forty 4 cm × 4cm × 4cm-cubes were obtained with disc-cutting finish (Fig. 2A).

2.2. Consolidants

Prior to the application of consolidants, thirty samples for each stone were subjected to 500 °C during 24 h and subsequently, they were shock cooled by tap water jet, simulating the effect caused by firefighters' intervention in a fire (Fig. 2B and C). Ten samples of each stone were kept without heating.

After the cooling down, the samples were kept at 40 °C during 2 days to ensure the drying, because according to [51], consolidants products should be applied in a dry stone to ensure a higher dry matter. Then, two different commercial nanoconsolidants products provided by CTS S.R.L. (www.ctseurope.com) were applied on the surface. Ten samples of each stone were coated with each consolidant:

- Nano Estel® (NE hereinafter) is an aqueous colloidal solution of nano-size silica particles (10–30 nm). Following technical sheet of this product, these particles are smaller than those found in acrylic microemulsions (40–50 nm) and nanolime (200 nm). The nano-size silica particles bind among themselves forming a silica gel, similarly to that obtained for ethyl silicate consolidants [52]. Considering suppliefs recommendations, since the commercial product is concentrate, it has to be diluted with 1–2 parts of deionized water. Therefore, considering the ruined substrates after heating at 500 °C, NE was directly applied. They ensured that three of four days are necessary to complete its polymerization at 20 °C.
- Nanorestore® (NR hereinafter) is a dispersion of $Ca(OH)_2$ hexagonal portlandite platelets of 250 nm in 2-propanol [30]. Following the technical sheet of this product, it was directly applied on the stones. If the product is diluted with 2-propanol or water, up to twelve applications are recommended. Moreover, five or seven days are considered the time enough to achieve the carbonation of the product.

For each stone, all the faces of each samples were treated with each consolidant product by brushing [53]. Since the heating could severely affect to the porous structure of the stone, the products were applied directly. After each application by brushing the samples were left to air dry (18 °C and 50%RH) until constant weight (approx. 20 days) and then, the Karsten pipe method following [54] was applied (Fig. 2D and E). A vertical pipe filled with 10 mL of distilled water was attached with plastiline to the surface of the stone and then, volume decrease was registered. Applications were performed until the volume decrease was equal or lower than that registered on the surface that was not subjected to 500 °C.

Therefore, for each stone, ten samples were kept unheated and unconsolidated, ten samples were heated and twenty samples were heated and consolidated.

2.3. Evaluation of the consolidation effectiveness, side-effects and durability

Firstly, dry matter content by measuring the difference of weight (%, w/w) was determined on each cube. Average value for each consolidant was calculated.

All the samples (unheated and unconsolidated samples, samples subjected to 500 °C and samples after heat and consolidation with both products) were also evaluated with stereomicroscopy (Nikon SMZ800).

In order to study the consolidation effectiveness, the following tests were performed to the unheated and unconsolidated stones, the surfaces subjected to 500 °C and the surfaces after high temperature and consolidation with both products:

- Firstly, the physical properties evaluated were: i) the water accessible porosity (open porosity, %) and the apparent density (ρ_b, kg/m^3) were determined in accordance with [55] ; ii) the coefficient of average absorption (AC, i.e. the slope of the linear part of the curve obtained by plotting *Qi* (mass change per unit area) in relation to the square root of time t(s)$^{1/2}$ following [56] and expressed as g/m^{2}s$^{0.5}$); and iii) the water absorption at atmospheric pressure (A_b %) was calculated using [57].
- Then, P-wave velocity (compressional wave velocity) was determined using the ultrasonic tester model Controls 58-E0048 with measuring range from 0.1 μs to 55.6 μs and accuracy of ±0.1 μs, using the transmission method, which consists of coupling two piezoelectric sensors on opposite faces of the sample for measuring the transit time for the ultrasonic pulse travelling through two opposite positions. The velocity was calculated following [45]. Six measurements of ultrasonic transit time were made per sample (two measures for facing faces).

Additionally, in order to study the side-effects of both consolidants on stones' surfaces, colour measurements were taken in CIELAB and CIELCH colour spaces [58,59] with a CM-700d Minolta spectrophotometer. For each sample, thirty random measurements were taken in a face of the cube in order to obtain results statically consistent for the granitic samples [60]. Despite Sanmartín et al. [61] reported that in stone less heterogeneous than the granite, less numbers of measurements are enough to determine the colour of the stone, the colour data collection was performed in the same way for both stones. Rivas et al. [62] stated that a number of measurements equal to or greater than that recommended following the granite texture, has a statistically no significant influence on the measurement of colour. The Cartesian parameter measured was the lightness (L*) varying from black (0) to white (100) and the polar coordinates a* from red (+a*) to green (−a*) and b* from yellow (+b*) to blue (−b*). In CIELCH colour space, L* was also included and in addition chroma, saturation or colour purity (C^*_{ab}) and the hue (h_{ab}) were obtained. The measurements were made in specular component included (SCI) mode, for a spot diameter of 8 mm, using illuminant D65 and with an observer angle of 10°. Then, colour differences (ΔL^*, Δa^*, Δb^*, ΔC^*_{ab}, ΔH^*) and global colour change (ΔE^*_{ab}) were computed taking the colour of the unheated and unconsolidated stones as the reference value for the colour change of the heated samples and this latter to detect the colour changes for the consolidated ones [58,59].

In order to chemically characterize the consolidants and determine their presence on the surfaces, the consolidants were dried for twenty days on microscope glass slides in the same environmental conditions (18 °C and 50% RH) and compared to the consolidated surfaces by means of Fourier Transform Infrared Spectroscopy (FTIR) in micro mode with a FTIR Thermo Nicolet® Continuum. The FTIR spectra were recorded in reflectance mode in the 4000 cm^{-1} to 400 cm^{-1}-region, with 4 cm^{-1} resolution.

Then, for each stone, surface fragments (approx. 1 cm × 1 cm × 1 cm) of the unheated and unconsolidated samples, surfaces subjected to 500 °C and surfaces subjected to 500 °C and treated with both consolidants, as well as the dried consolidants after twenty days applied on microscopy glasses, were observed by Scanning Electron Microscopy (SEM) using a Philips XL30 coupled with an energy dispersive X-ray spectrometry (EDS) (Oxford Inca Energy 300 SEM) in secondary electrons (SE) and backscattered electrons (BSE) modes. Carbon-coated samples were visualized at an accelerating potential of 15–20 kV, a working distance of 9–11 mm and specimen current of ~60 mA. SEM allowed to find the composition of the dried consolidants and the distribution and morphology of both consolidating products on the surfaces.

Finally, the durability of the consolidants was evaluated by studying the resistance of all samples to salt crystallization cycles according to [63]. As it was reported in previous studies [64,65], the artificial ageing tests, such as salt crystallization, give more realistic results about the effectiveness of consolidants products since the amount of absorbed consolidants for these stones is low. The determination of bulk properties, such as water accessible porosity, did not give reliable information about the improvement in the stone cohesion. Samples were subjected to fourteen salt crystallization cycles; each cycle (24 h) was based on i) 2 h of capillary absorption of a sodium sulphate solution at 14% (w/w), ii) an oven drying at 105 °C during 20 h, iii) cooling at 18 °C and 50% RH during 2 h. At the end of 14 cycles, the samples were washed in a bath of distilled water at 20 °C until their weights were constant. The resistance to the salt crystallisation was measured from the weight change (Δm, %) after the test. After salt crystallization test (14 cycles), samples were evaluated through the determination of open porosity (%), stereomicroscopy, FTIR and SEM.

3. Results and discussion

3.1. Evaluation of the consolidation effectiveness and side-effects

In Table 1 is presented the number of application of consolidants following Karsten pipe method, the dry matter (%, w/w) of each consolidant for both stones and the physical characterization of the samples.

Comparing both references, the granite had higher open porosity than the limestone, even before to be exposed to 500 °C. The obtained values are in agreement with previous researches [65,66]. The open porosity of the granite is associated to the Hercynian orogeny ranged from 2% to 4% [65,67]. However, post-hercynian granites such as *Rosa Porriño* and *Rosavel* showed open porosity slight lower, lower than 1.2% [68]. Regarding to the limestone, Lioz commonly showed open porosity lower than 0.5% [66]. After the exposure to 500 °C, both stones exhibited an increase of

Table 1
Number of applications of each consolidant to the heated stones (500 °C), dry matter and physical test results for reference stones, samples subjected to 500 °C and the consolidated samples. Open porosity (%) was determined before and after 14 salt crystallization cycles. NE: Nano Estel® and NR: Nanorestore®.

Stone	Condition	N° of applications	Dry matter (% w/w)	Open porosity (%) before 14 salt crystallization cycles [55]	Open porosity (%) after 14 salt crystallization cycles [55]	Apparent density (ρ_b, kg/m^3) [55]	Water absorption by capillarity AC (g/m^{2}s$^{0.5}$) [56]	Water absorption at atmospheric pressure A_b (%) [57]
Granite	Reference	–	–	3.89 ± 0.10	5.23 ± 0.18	2727.56 ± 64.77	148.75 ± 14.07	2.21 ± 0.70
	500 °C	–	–	6.49 ± 0.53	6.53 ± 0.42	2689.20 ± 47.02	231.25 ± 22.13	2.61 ± 0.64
	500 °C + NE	8	0.778 ± 0.006	4.92 ± 0.74	5.81 ± 0.15	2700.32 ± 50.71	39.50 ± 2.03	1.92 ± 0.09
	500 °C + NR	5	0.760 ± 0.195	4.60 ± 0.74	5.65 ± 0.13	2710.96 ± 70.09	64.85 ± 0.21	2.12 ± 0.49
Limestone	Reference	–	–	0.25 ± 0.10	0.94 ± 0.22	2880.76 ± 51.98	5.95 ± 0.98	0.29 ± 0.04
	500 °C	–	–	2.32 ± 0.37	2.38 ± 0.71	2834.51 ± 74.17	63.41 ± 3.74	1.62 ± 0.03
	500 °C + NE	3	0.221 ± 0.027	2.52 ± 0.46	3.26 ± 0.02	2814.06 ± 55.92	48.55 ± 8.70	0.96 ± 0.01
	500 °C + NR	3	0.018 ± 0.006	2.57 ± 0.48	2.85 ± 0.27	2815.99 ± 51.40	68.20 ± 2.69	0.99 ± 0.06

the open porosity, being slightly higher for the granite. In both stones, this increase of open porosity is associated to the fissures occurred after the heating and cooling down. Vázquez et al. [69] found that at 400 °C, mica sheets opened due to the expansion and contraction processes and quartz grains showed cracks. After 600 °C, feldspars also showed a crack development [68–70]. Regarding the other physical properties, capillary absorption coefficient (AC) and water absorption at atmospheric pressure (A_b) also experimented increases with statistically significant differences comparatively to the unheated stone, except for A_b of the granite. The generation of new microfissures and cracks due to expansion-contraction of forming minerals is the responsible process to increase the cited physical properties after heating [45,71–74]). Additionally, in limestone, calcite which is the main mineral for those stones, expands and contracts in different directions as calcite crystals are strongly anisotropic if compared with other minerals [75]. Calcite minerals are disruptive even at low temperatures, and then significant increases of open porosity and capillary absorption coefficient were observed after heating. The volume increase of calcite grains induces the formation of micro-fissuring and intra and intergranular pores [45,72,76]. In the case of a compact and low porous stones (i.e. the studied limestone), the increase of the open porosity is higher than that found in other fissured stones such as granite, due to the lack of intergranular voids to support the thermal expansions of the mineral grains [71,73,74].

Considering the consolidated samples, the dry matter was higher on the granite, due to the higher number of applications required for this stone compared to the limestone treatments. In the case of the granite, higher number of NE applications (eight applications) were needed comparatively to the NR (five applications). Despite the number of applications, both consolidants obtained similar dry matter values in this stone (approx. 0.780 %w/w for NE and 0.760 %w/w for NR). Similar dry matter values were detected in other researches working with ethyl silicate consolidants applied on granites [51]. On the other hand, in the case of the limestone, regardless of the consolidant applied, three applications were needed. Limestone samples treated with NE obtained higher dry matter values compared to samples treated with NR (approx. 0.221% w/w for NE and 0.018% w/w for NR), which suggests that limestone treated with ethyl silicate present a higher amount of consolidant in the pores compared to the nanolime samples. This could be attributed to the low open porosity and fine pore structure of the Lioz limestone (as shown in Fig. 1B), which could have limited the access of the NR particles in the pores. Recent studies suggested that NR tends to close primarily pores with large pore size diameter (~600 nm) being not very effective in the finer pores structure (pores with diameter size <600 nm) [44]. This is attributed to the NR particle size (~150–300 nm) and the clusters of nanoparticles size (~600 nm) formed after the nanoparticle agglomeration phenomenon [31,44], which seems to limit the access of them into a fine pore structure (<600 nm). The smaller particle size of the NE (~10–30 nm), compared to NR (~150–300 nm), might have allowed a better penetration into the finer pore structure of the Lioz limestone. Martinho et al. reported similar dry matter deposited of NR working on the same limestone; specifically, 0.065% [45].

After consolidation, open porosity was reduced in the granite stones for both consolidation treatments (approx. 24% for NE and 29% for NR), comparatively to the heated sample. However, in the limestone, open porosity values of the consolidated stones were similar to the heated stone. This could be attributed to the lower number of applications carried out in the limestone (3 applications) compared to the granite samples (5 and 8 applications). In previous researches, Martinho et al. [45] did not find also an increase of open porosity in the limestone heated at 600 °C coated with NR, suggesting that this consolidant showed lower effectiveness than the ethyl silicate consolidant Tegovakon® [45]. Other work [77] yielded similar decreasing values of the porosity for the samples treated with TEOS, which was the most effective, lowering the capillary porosity, especially in respect of the smallest capillary pores (1–0.01 μm). Additionally, other works also found that NR caused just a small closing of the pores in the surface area [78,79].

AC and A_b indexes showed significantly decreasing values comparatively to those of the heated samples for both treatments in granite stone (AC ~66% for NE and 72% for NR). This decrease of the water absorption by capillary is due to a reduction of the porosity on the granite's surface, which slows down the capillary rise [80]. These results are in accordance to the open porosity results reported above, which suggest that both treatments in granite yielded higher reduction on porosity. In contrast, results of the limestone samples showed that NE caused a small reduction of the AC and A_b values (AC ~23% reduction), while NR samples showed similar AC and A_b values to the heated samples. This might be attributed to the lower presence of the nanolime consolidant in the limestones, which was described above. In agreement with [81] the nanosilica consolidant NE reduced the porosity of both stones which become more compact. Therefore, the samples will be less susceptible to deterioration mechanisms related to the action of water, such as salt crystallization.

Measurement of water absorption by capillary rise shows that, after heating, both stones showed a greater increase in water absorption because of the coarser pores with a diameter 0.1–100 μm, which present higher capillary suction [80,82]. After consolidation, the capillary suction kinetics of the granite samples significantly decreased obtaining lower CA than the unheated sample-reference (Fig. 3A). Granite samples treated with NE obtained higher decrease compared to the samples treated with NR, despite both obtained similar decreasing values of porosity. This suggests that NE treatment could be more effective protecting against the water capillary absorption due to the hydrophobic effect of the ethyl silicate, which has been reported by several authors working with stones [83] and concrete [84]. However, for the limestone, the sample with NE experimented a small decrease in water absorption, which is related to the slight reduction of the porosity on this stone after treatment. Conversely, the NR samples showed no significant reduction of the water absorption by capillary curves. In this stone, the first part overlaps with the curve of the heated sample (Fig. 3B). These results are in the line with the results of open porosity and dry matter reported above, where it is shown that nanolime is less effective in the limestone due to the lower presence in the pores.

Ultrasonic wave method has been useful to qualitatively investigate the penetration depth of the consolidant product in stone material [45]. The p-waves velocity in a solid depends on the density and elastic properties of the material [45,85]. The different materials forming the sample contribute to the final p-wave velocity proportionally to its volume [45,85]. In Fig. 4, it is shown the p-waves velocities for the all samples tested. Higher values were registered in the limestone compared to the granite, which is clearly related to the lower porosity of this stone compared to the granite stone. Vazquez et al. [86] working with other granites from NW Spain, with lower open porosity (ranges 0.94–1.12%) than the selected granite, obtained p-waves velocity higher than 4400 m.s^{-1}, showing the low cracking intensities of these granites comparatively to the one used in this research. However, p-waves velocity detected in the limestone is an indicative of the high presence of cracks in this stone since in the Lioz limestone the p-waves average velocity ranged 6500–7000 m.s^{-1} [45]. However, limestone samples present lower amount of cracks comparatively to the granite.

After heating, both stones showed an important decrease of the p-waves velocity, which is clearly related to the increase of porosity induced by the heating process. This result is in agreement with [45]; after 600 °C, they reported that for Lioz, p-waves velocity experimented a significant decrease (more than 50% comparatively to the reference stone) with average values between 3500 and 2500 m.s^{-1}. In the current case, the p-waves velocity was notable lower that those values, because the p-waves velocity for the heated Lioz at 500 °C was 1980 ± 70.01 m.s^{-1}. Note that the unheated samples already showed values lower than those reported by Martinho et al. [45] and also, these authors exposed the samples to 600 °C, while in the current study, the samples were exposed to 500 °C. However, Martinho et al. [45] also reported that in several areas of the specimen, the velocity was lower than 1500 m.s^{-1}.

After the consolidation, the behaviour registered for the granite shows that both consolidants increased the p-waves velocity, which is due to the decrease of the porosity after both treatments. Conversely, in the limestone, both treatments only obtained a slight increase of the p-waves velocity, which is attributed to the low changes on the porosity, suggesting that both treatments did not affect massively the pore structure. These results are in the line with the dry matter and porosity results showing that the porosity after both treatments did not changed (Table 1).

Fig. 5 shows stereomicrographs of the stone surfaces. In the unheated and unconsolidated granite, features of typical forming minerals surfaces can be identified (Fig. 5A): conchoidal fracture of translucid quartz minerals, whitish feldspar and plagioclase grains, black-greenish exfoliation planes of biotite grains and an orange-yellowish colouration affecting the areas around the biotite grains, staining the leucocratic minerals (K-feldspar and plagioclase grains) related to the existence of iron forms filling the fissures of these minerals [47,87]. Note that this yellow colouration must be considered as a characteristic textural feature of this stone. After 500 °C, this orange-yellowish colouration was transformed in a reddish stain, filling fissures in the leucocratic minerals (Fig. 5B), as was reported in previous researches [88,89]. The change of the yellowish colouration to the reddish colouration would be due to the transformation of goethite to hematite. Pozo-Antonio et al. [89] reported that, in a prehercynian granite which was collected in a petroglyph site with similar mineralogy and texture, the change from yellowish to reddish tones due to the transformation to hematite of the Fe oxyhydroxides present in the granite fissures.

However, limestone was not as affected as the granite after 500 °C and only a slight brown colouration was found in the heated surface (Fig. 5E and F). Dionísio et al. [90] also explained the colour changes in this stone after firing with the iron oxide-oxyhydroxides transformation from goethite to hematite.

After consolidation, in the granite surface coated with both nanoconsolidants, it was possible to find a shining translucid veil on the surface (Fig. 5C and D). Moreover, in the surface covered with NE, a yellow coloured stains covering indistinctly the differ-

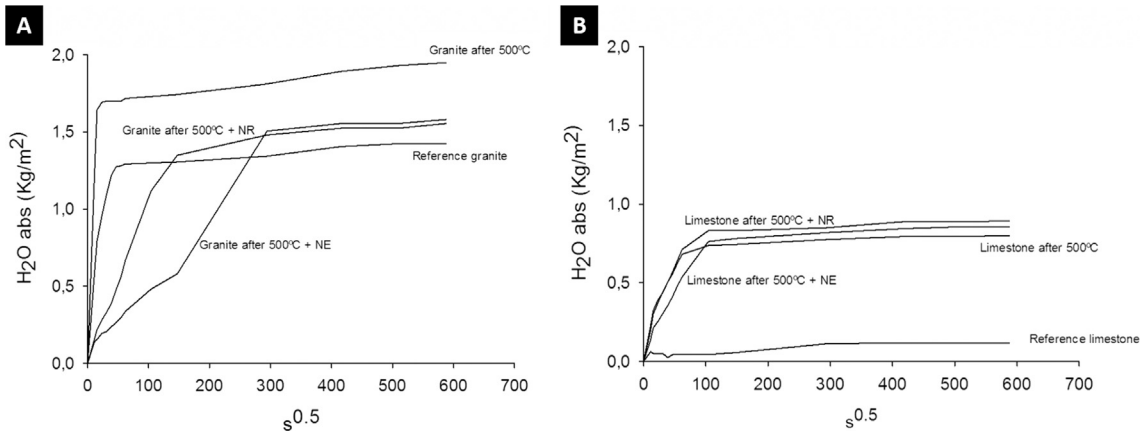

Fig. 3. Capillary absorption curves for granite (A) and limestone (B): unheated and unconsolidated samples, heated samples and consolidated samples with NE and NR. NE: Nano Estel® and NR: Nanorestore®.

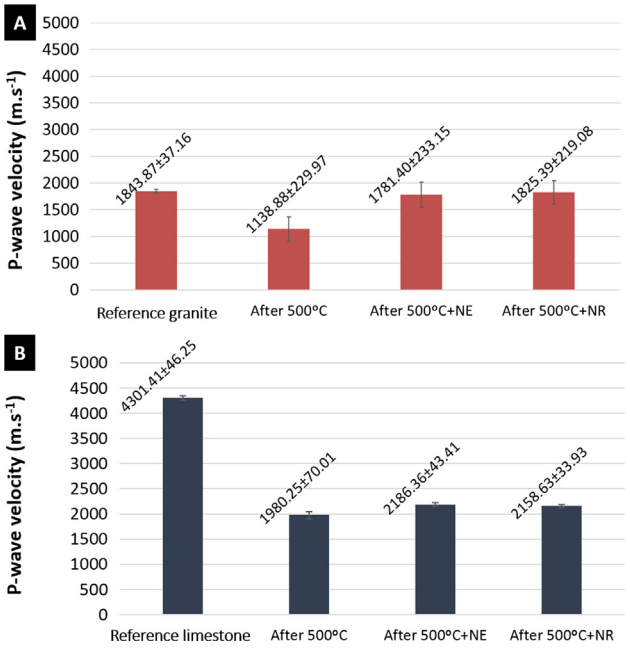

Fig. 4. Results of the measurement of the p-waves velocities ($m.s^{-1}$) for the granite samples (A) and limestone samples (B). NE: Nano Estel® and NR: Nanorestore®.

ent forming minerals were detected (Fig. 5C – detailed micrograph). In the granite samples treated with NR, the shining translucid veil showed some whitish colouration effects (Fig. 5D). Borsoi et al. [91] also detected a yellowing effect on historical renders. Zornoza-Indart et al. [46] working on a calcarenite with a nanostructured consolidant composed by a silica oligomer precursor Wacker TES 40 WN® with the addition of n-octylamine as a surfactant developed by Illescas et al. [92], found also a marked yellowing. In the limestone, effects assigned to the coatings on the surface were not detected (Fig. 5G and H), which probably is due to the lower amount of application and thus the lower presence of both consolidants in the limestone samples. In two different stones (a limestone and a sandstone), Musacchi and Diaz-Gonçalves [25] found that the nanolime CaloSil® (colloidal solution of nano-calcium hydroxide in ethanol), similar in composition to NR, gave a whitish tone to the surfaces and the NE gave them some shining effect. Both commercial nanolime consolidants, NR and CaLoSiL E15®, were tested on several substrates (wall paintings, lime mortars and limestone) reporting a clearly visible formation of white haze, immediately after alcohol evaporated [43,44,79,93]. The whitish colouration was explained by Musacchi and Diaz-Gonçalves [25] with the deposition of calcium hydroxide particles after alcohol evaporation. Then, these particles were transformed into calcium carbonate by reaction with the CO_2. However, the penetration and deposition of the nanoparticles in the pores of the limestone still needs to be fully understood, and its effects on the whitish colouration on the surface after treatment. Conversely, some other authors [30,94,95], stated that NR caused almost no aesthetical alteration of the colour of the substrate. Baglioni et al [30] reported that the application of calcium hydroxide particles on a wall painting coming from the archaeological Maya site of Calakmul (Campeche, Mexico) did not induce any visible colour change, despite a global colour change of 4.2 CIELAB units was computed. Note that 3.5 CIELAB units is the ΔE^*_{ab} threshold showing that an inexperienced observer can notice the difference [96].

Colour spectrophotometry detected that after heating, the granite was the stone that showed the highest change of the surficial colour (see Table 2); ΔE^*_{ab} of the granite after heating is higher than 3.5 CIELAB units, which is the ΔE^*_{ab} threshold to show a noticeable colour change by the naked eye [89]. In silicate stones, noticeable aesthetic damage begins to take place at temperatures lower around 300 °C, being the main contributor to this change the modification associated to the iron thermal oxidation which occurs between 205 °C and 300 °C [6,68,70]. This is reflected in the coordinate a* which is the parameter more affected by the global colour change, showing an increase higher than 3 CIELAB units. Vazquez et al. [68] reported that for granitoids at 400 °C, colour varies strongly in yellow granites, from yellow to red tones. In the heated limestone Lioz, the ΔE^*_{ab} was not visibly detected by the naked eye, because it was lower than 3.5 CIELAB units [96]. However, b* was the colour parameter more affected by the heating showing a decrease, which is related to the brown colouration as result of the iron oxide-oxyhydroxides transformation from goethite to hematite [90].

After consolidation, in both stones, NE is the consolidant that obtained the highest ΔE^*_{ab}, mainly on the granite sample (Table 2). Note that yellow coloured stains covering the surfaces were detected by stereomicroscopy in the granite. NE on ignimbrite samples induced lower variations than the ethyl silicate consolidant Estel 1000® and Estel 1100®, but the more the NE concentration the more the ΔE^*_{ab} [39]. This effect was also showed in [77]. Note that in the current research, NE was directly applied without any dilution. NR also induced a noticeable detected colour change in the granite ($\Delta E^*_{ab} > 3.5$ CIELAB units), while in the limestone, NR treated surfaces showed ΔE^*_{ab} lower than 1 CIELAB unit, being this colour change undetectable by the naked eye [96]. In previous works, nanolime was found to change the aesthetic properties due to a whitening surface on top [13,31,77]. Conversely, other researchers found no aesthetic changes after the application of a nanolime treatment [30,32]. In a previous research [52], NE and a 2-propanol dispersion of $Ca(OH)_2$ as NR were applied on the biocalcarenite Lecce Stone and it was found that this stone was very poorly affected by treatments with nanoparticles because ΔE^*_{ab} lower than 2 CIELAB units were obtained. However, the application of tetraethoxysilane Estel 1000 in white spirit induced more considerable chromatic changes: $\Delta E^*_{ab} > 3.5$ CIELAB units [52].

Considering the compatibility criteria following [97], the colour differences obtained after the application of NE on both stones and NR on granite are considered as high ($\Delta E^*_{ab} {}^* > 5$), while NR on limestone shows a low risk of incompatibility ($\Delta E^*_{ab} {}^* < 3$).

In granite, after the consolidation with both products, the more affected coordinate was L* (Table 2) as was reported in [93] working with nanolime on wall paintings. A darkening ($-\Delta L^*$) of the surfaces was detected being higher in the surface with NE. Pondelak et al. [93] found that the colour differences are due to a darkening ($-\Delta L^*$) for grey coloured stones or a slight lightening ($+\Delta L^*$) in the case of the substrate with a red colouration. In the current research, the general colour of the surfaces was closer to grey colour. The colour of granite with NE also experimented a slight b* increase suggesting a yellowing of the surface. This is in agreement with stereomicroscopy because it was identified yellow stains on the surface (Fig. 4C – detailed micrograph). In limestone, as was reported for the granite, the global colour change of the surface coated with NE was mainly affected by a darkening of the surface, while in the sample with NR, the changes of the parameters L* and b* were similar, being slightly higher for the b* coordinate. In fact, the b* increase suggests a yellowing of the surface.

FTIR spectra of the powder consolidants allowed to identify the representative IR bands (reflectance) of each product (Fig. 6). FTIR spectrum of the NE is characterized by a shoulder at 1165 cm^{-1} assigned to silica gel Si–O ν_3 vibrations, a low intense shoulder a 1000 cm^{-1} due to the Si-O stretching vibrations in residual silanol groups and a band at around 830 cm^{-1} associated with Si–O ν_1 vibrations [18,98]. The existence of silanol suggests that the poly-

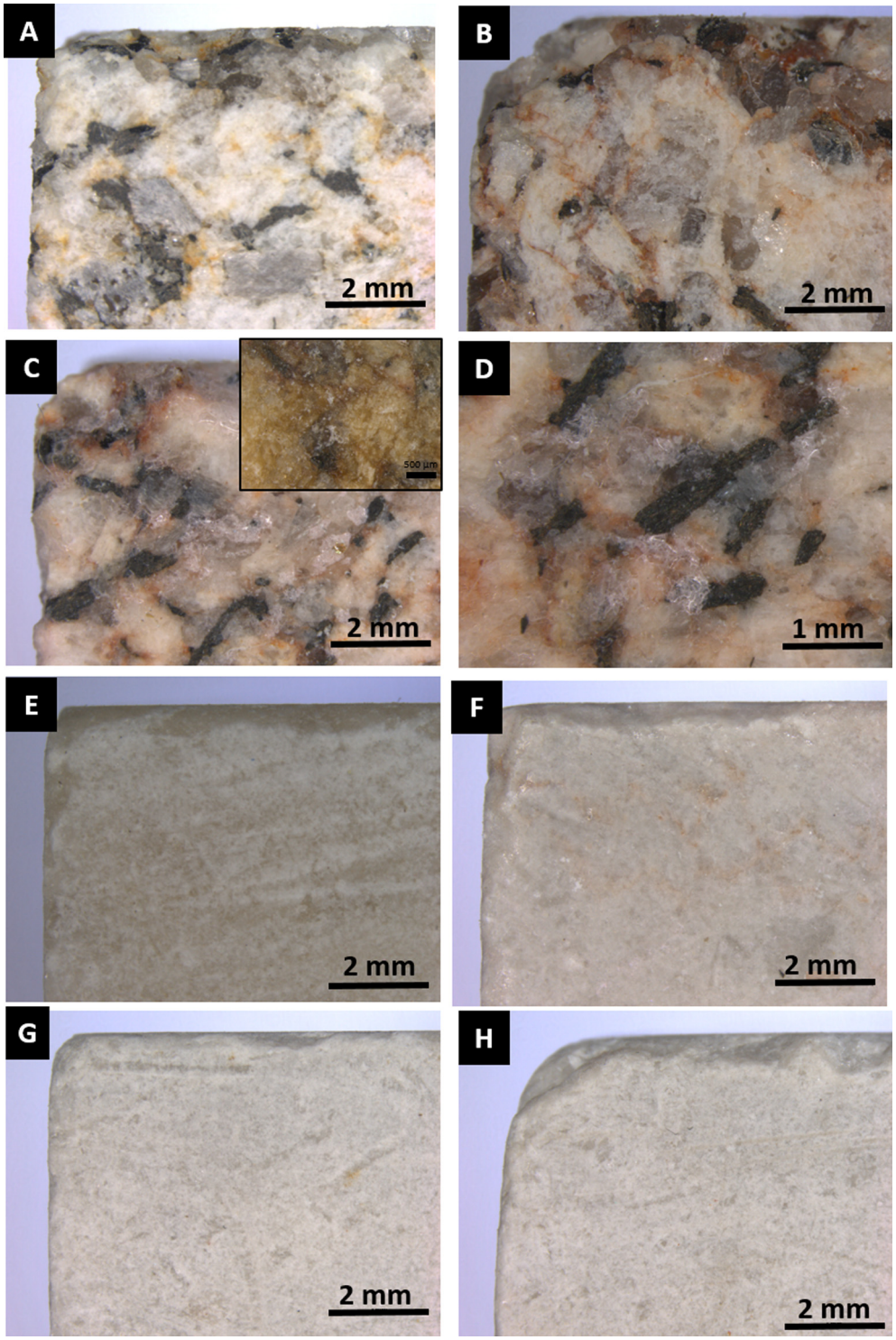

Fig. 5. Stereomicrographs of the granite samples (A-D) and the limestone samples (E-H). A and E: reference samples (unheated and unconsolidated surfaces). B and F: stones after 500 °C without consolidants. C and G: samples consolidated with NE. D and H: samples consolidated with NR. NE: Nano Estel® and NR: Nanorestore®.

merization was not fully completed despite C–H stretching vibrations bands at 2929 and 2852 cm^{-1} were not find. Note that the consolidation action is due to the hydrolysis and condensation reaction leading to a silica gel inside the pores of the materials [83]. Hydrolysis and condensation take place because of the reaction of ethyl silicate and atmospheric moisture [99].

The final product after complete polymerization process of the ethyl silicate is about three weeks [100].

FTIR spectrum of the NR showed the characteristic reflectance bands of this kind of products [101,102]: at 3690 cm^{-1} assigned to O–H stretching vibrations by calcium hydroxide suggesting that the nanolime was not fully carbonated after 20 days at room conditions (18 °C and 50%RH). Moreover, bands also detected were the broad band at 3350 cm^{-1} assigned to O–H stretching vibrations generated by water, 2929 and 2852 cm^{-1} assigned to C–H stretching vibrations and 2540 cm^{-1} assigned to water stretching. $CaCO_3$

Table 2
Colorimetric coordinates L*, a*, b*, C^*_{ab} and h_{ab} for the unheated and unconsolidated (reference) samples, the heated surfaces at 500 °C and the consolidated ones. Standard deviations are also shown (n = 150). Colorimetric differences and global colour changes ΔE^*_{ab} were computed for the heated surfaces and the consolidated stones, comparatively to the unheated and unconsolidated (reference) surfaces and the heated surfaces respectively. ΔE^*_{ab} higher than 3.5 CIELAB units shows that these colour variations are enough to be perceived by a human eye [96]. NE: Nano Estel® and NR: Nanorestore®.

Granite						
Sample	L*	a*	b*	C^*_{ab}	h_{ab}	
Reference surface	75.79 ± 1.86	1.65 ± 0.43	7.77 ± 1.07	7.95 ± 1.12	78.14 ± 1.53	
After 500 °C	73.36 ± 3.90	4.77 ± 1.32	8.63 ± 1.29	9.84 ± 1.67	61.37 ± 5.14	
After 500 °C + NE	65.11 ± 4.18	5.67 ± 0.99	10.04 ± 1.46	11.56 ± 1.50	60.48 ± 4.49	
After 500 °C + NR	68.30 ± 4.00	5.06 ± 0.74	9.17 ± 1.19	10.49 ± 1.23	61.05 ± 3.78	
Sample	ΔL^*	Δa^*	Δb^*	ΔC^*_{ab}	ΔH^*_{ab}	ΔE^*_{ab}
After 500 °C	−2.43	3.12	0.86	1.89	−2.58	4.05
After 500 °C + NE	−8.25	0.89	1.42	1.73	−0.14	8.42
After 500 °C + NR	−5.06	0.29	0.54	0.65	−0.05	5.09
Limestone						
Sample	L*	a*	b*	C^*_{ab}	h_{ab}	
Reference surface	80.99 ± 1.91	1.45 ± 0.17	6.34 ± 1.34	6.50 ± 1.34	76.92 ± 1.37	
After 500 °C	80.29 ± 1.02	0.89 ± 0.09	3.98 ± 0.55	4.08 ± 0.55	77.26 ± 1.25	
After 500 °C + NE	74.08 ± 1.66	1.35 ± 0.12	5.21 ± 0.49	5.38 ± 0.49	75.39 ± 0.97	
After 500 °C + NR	79.78 ± 1.16	1.06 ± 0.21	4.74 ± 0.87	4.71 ± 0.83	77.38 ± 0.75	
Sample	ΔL^*	Δa^*	Δb^*	ΔC^*_{ab}	ΔH^*_{ab}	ΔE^*_{ab}
After 500 °C	−0.70	−0.56	−2.35	−2.42	0.03	2.52
After 500 °C + NE	−6.21	0.46	1.22	1.30	−0.19	6.35
After 500 °C + NR	−0.51	0.17	0.76	0.63	0.01	0.93

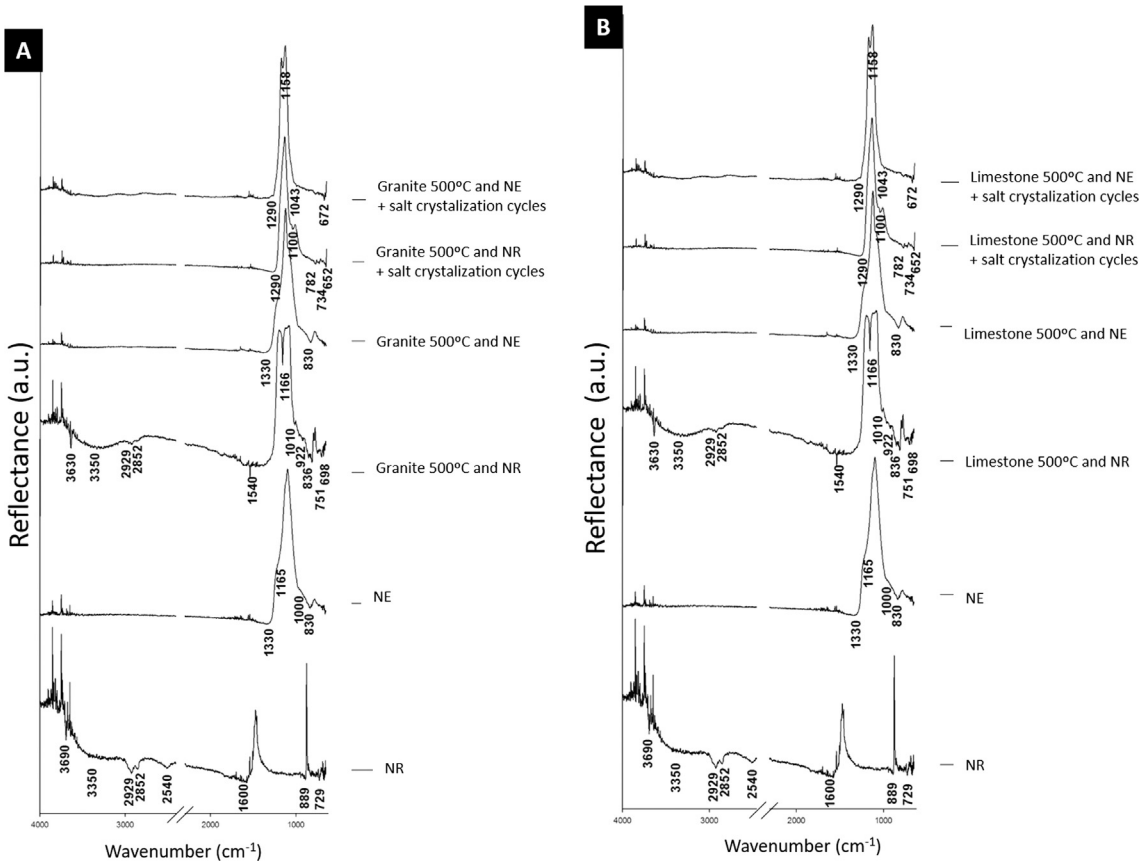

Fig. 6. FTIR (reflectance) spectra collected on nanoconsolidants powder, the stones consolidated and the coated samples after fourteen salt crystallization cycles. A: Granite samples. B: Limestone samples. NE: Nano Estel® and NR: Nanorestore®.

polymorphs, such as calcite and vaterite, can be identified through their representative bands at C–O v_2 in the range 875–830 cm^{-1} and O–C–O v_4 bands at 750–712 cm^{-1} [103]. Other researchers also found the presence of polymorphs of calcium carbonate after the carbonation of nanolime products [78,79,101].

On the consolidated surfaces, those treated with a consolidant with the same chemical composition as the stone, it was not possible to confirm the existence of the consolidant on the surface because the FTIR spectra were overlapped (Fig. 5). In FTIR spectra of the granite treated with NR (Fig. 5A), it was possible to observe

the presence of the consolidant through the bands assigned to the product. In case of the NE on the limestone (Fig. 5B), nanoconsolidant particles were detected through a remarkable decrease of the bands at 1429 cm^{-1}, which is the representative calcite band assigned to C–O v_3 stretching vibrations [98]. Moreover, the shoulder at 1165 cm^{-1}, the low intense shoulder a 1000 cm^{-1} and the band at around 830 cm^{-1} confirm the presence of the nanosilica consolidant [18,98].

Regarding the morphology and distribution of the consolidants on both stones, it is necessary to study the texture and mineralogy of the stones after heating and the morphology and composition of each consolidant by themselves (Fig. 7).

In case of both stones, after 500 °C, SEM showed that both stones increased the fracture level and fissures length (granite: Fig. 7A and B; limestone: Fig. 7D and E). In case of the granite, mainly on the sample subjected to high temperature, deposits rich

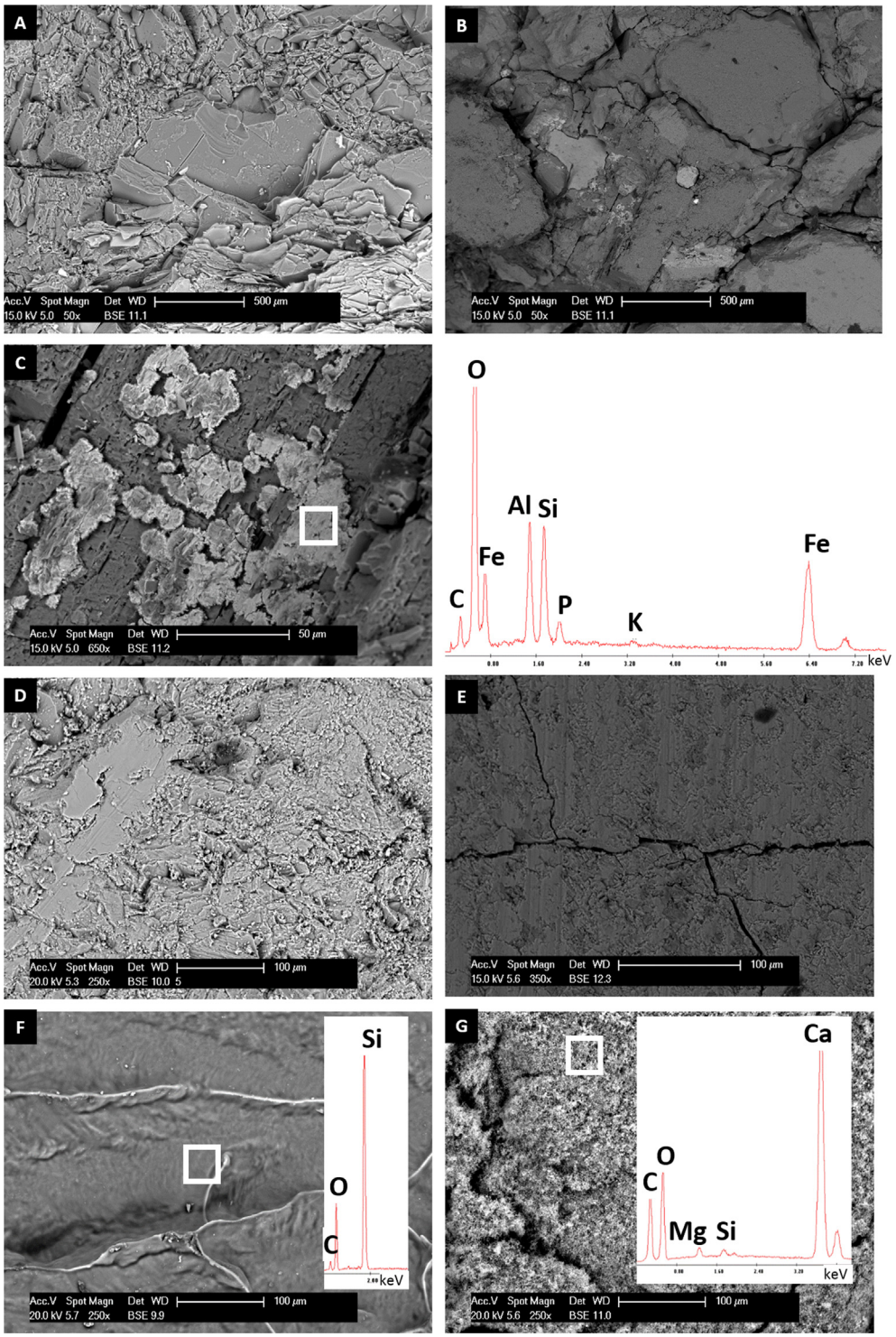

Fig. 7. SEM micrographs of some of the samples. A: reference granite. B-C: granite exposed to 500 °C during 24 h and cooled down with tap water. C is accompanied with the EDS spectrum of deposits found on the surfaces of the heated surface. D: reference limestone. E: limestone exposed to 500 °C during 24 h and cooled down with tap water. F: NE on a microscope glass and its EDS spectrum. F: NR on a microscope glass and its EDS spectrum. NE: Nano Estel® and NR: Nanorestore®.

in Fe, Al, Si and P were found on the felsic minerals (feldspar and plagioclase). These deposits were identified as Fe oxyhydroxides forms present in the granite, as results of the oxidation of Fe in biotite with the loss of Si, Mg, Ca, Mn, K, and Na [104]. Subsequently, Fe occurs in aggregates of microcrystalline aluminum-rich particles occurring as arrangements of crystals of goethite, gibbsite and hematite [104]. The deposits found in the heated granite presumably were hematite grains due to the transformation of goethite to hematite after the heating; the formation of hematite from goethite occurs within a wide temperature range that starts at around 300 °C [105].

SEM micrographs of the dried consolidant product on a microscope glass after twenty days allowed, in addition to know their composition, the identification of their morphological and microstructural features (Fig. 7F and G). NE shows an irregular dense coating rich in Si (Fig. 7F). NR shows a layer composed of nano plate-like particles rich mainly in Ca (Fig. 6G). Wen et al. [106] and Licchelli et al. [52] ascribed them to $CaCO_3$.

In the treated surfaces (granite: Fig. 8 and limestone: Fig. 9), SEM observation of the surfaces allowed to identify that, regardless of the stone, NE formed a homogeneous, thick and compact consolidation film, with large plate-like agglomerates of colloidal silica (Fig. 8A and Fig. 9A, B) with a few μm of thickness (Fig. 8B and Fig. 9C). As known, nanosilica is a wet gel with nanometer-scale oxide particles, surrounding an interconnected network of pores that are filled with fluid, typically the solvent, which is water for NE [107]. The evaporation of the water leads to pores collapse and a highly densified xerogel is obtained [107]. Therefore, nanosilica tends to shrink and to detach from the surface, forming wide cracks and fissures. In this sense, the durability of the consolidation treatment and its penetration depth can be reduced [91]. After SEM visualization of the cross section, it was observed that, regardless of the consolidant, in granite, the penetration was higher than in the limestone, since it was possible to observe polymerized and carbonated product through the fissures (Figs. 8B and 9C). The higher open porosity and the fissure system of granite contributed to the higher penetration recorded in the granite. The porosity of granite is characterized by transgranular fissures which are connected by microfissures, being responsible for the water absorption by

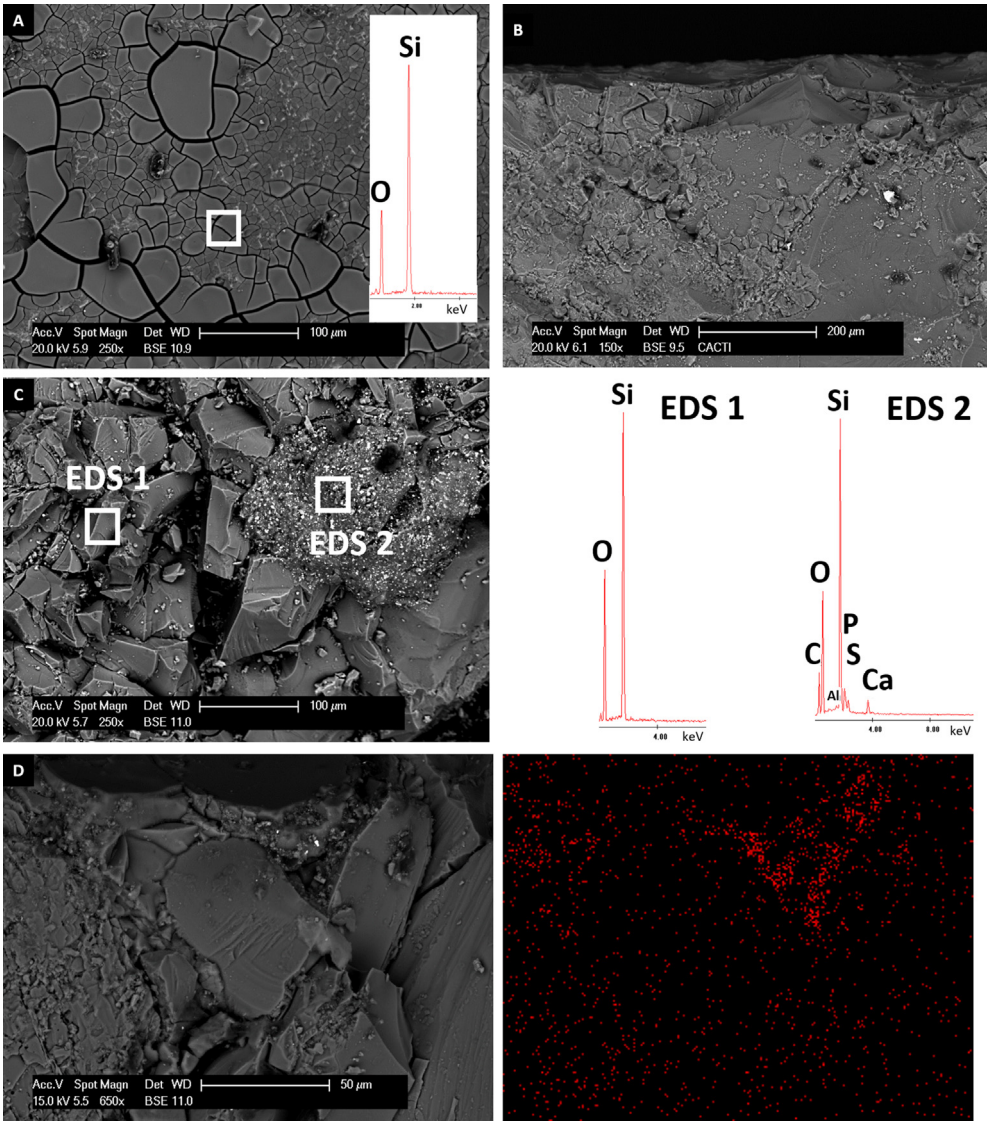

Fig. 8. SEM micrographs of granite samples consolidated with both nanoconsolidants. A: granite surface consolidated with NE accompanied with EDS spectrum. B: cross-section of the stone consolidated with NE. C: granite surface consolidated with NR accompanied with EDS specta. D: cross-section of the stone consolidated with NR accompanied with Ca content map. NE: Nano Estel® and NR: Nanorestore®.

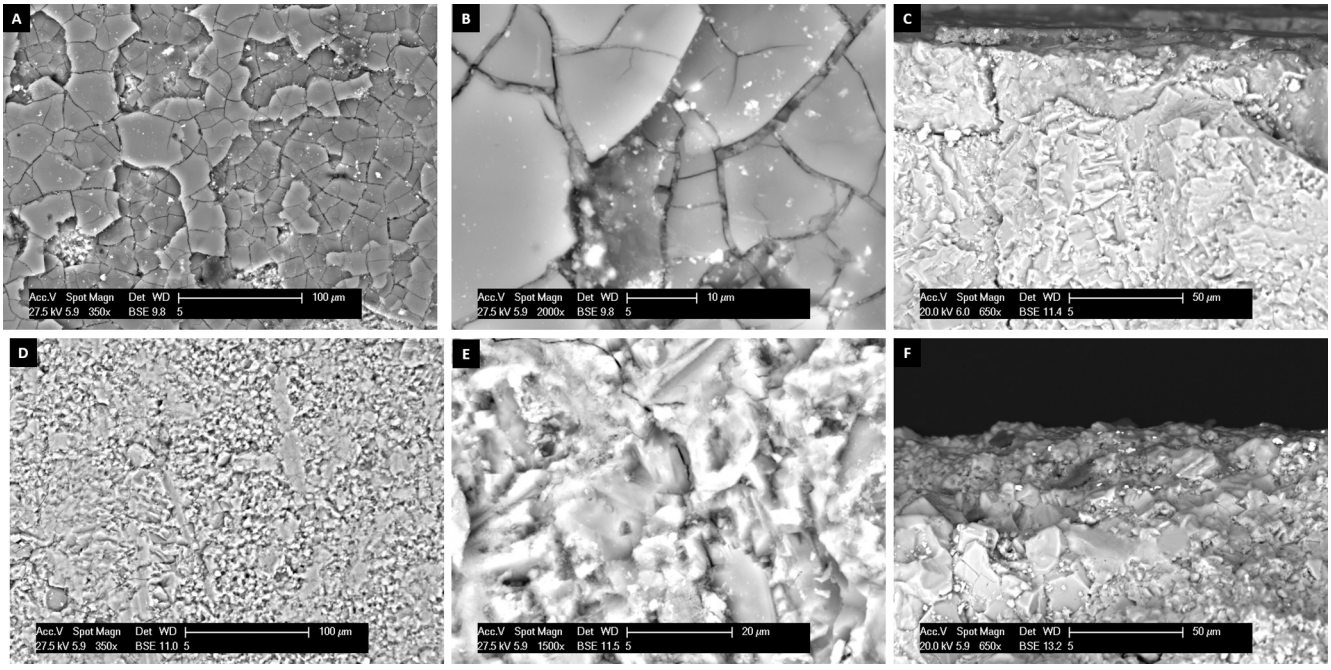

Fig. 9. SEM micrographs of limestone samples consolidated with both nanoconsolidants. A-B: surface consolidated with NE accompanied. C: cross-section of the stone consolidated with NE. D: limestone surface consolidated with NR. F: cross-section of the stone consolidated with NR. NE: Nano Estel® and NR: Nanorestore®.

capillarity [82]. In the limestone, NE was shown as a surficial layer without penetration (Fig. 8C).

Regarding to the nanolime, NR created a discontinuous deposit on the granite, recognized due to their morphology and their EDS analysis (Fig. 7C). Different crystalline polymorphs and amorphous phases of $CaCO_3$ were obtained in the granite. Different polymorphs of $CaCO_3$ can obtained after the carbonation of calcium hydroxide depending on relative humidity, temperature and CO_2 concentration [106,108]. However, in the limestone, it was not possible to distinguish the presence of nanolime in the stone. This could be attributed to the lower presence of this product in the limestones and due to the same mineralogical composition of nanolime and substrate. Considering the accumulation accumulation of NR, as was reported in the case of the granite, the nanoparticles were found in valleys on the surface (Fig. 9D and E). Despite the penetration of NR in the granite seemed to be less than that for NE, Ca-rich particles associated to the product were found through the fissures (Fig. 8D: SEM micrograph and Ca-map with EDS). However as was reported by the NE, it was not possible to identify NR penetration in the limestone (Fig. 8F).

3.2. Durability of the consolidants on the stone

During the salt crystallization cycles, it was observed that heated stones (Figs. 10B and 11B) experimented a higher loose of mass (%) compared to the unheated stones (Figs. 9A and 10A). The maximum mass loss was detected after the sixth cycle, regardless if the stone was heated or unheated. The mass loss is attributed to the first loss of material due to the existence of new fissures. After this cycle, the stone started to gain mass and therefore, $-\Delta M$ (%) started to decrease. La Russa et al. [39] also reported an increase in weight due to the salt precipitation inside the pore structure. However, for the treated samples the behaviour of the stones was different considering the consolidant used. In the granite, despite both consolidants allowed the reduction of mass loss comparatively to the heated stone, NR allowed the lowest mass reductions (Fig. 10D), while NE seemed to protect the limestone against the mass loss due to salt crystallization cycles (Fig. 11C).

After 14 salt crystallization cycles, the open porosity of the samples was obtained (Table 1). All samples increased the open porosity after cycles, as expected. It was detected that in the unheated and unconsolidated samples, the open porosity after the salt crystallization cycles experimented an increase. In the case of granite, the unheated samples yielded significantly higher increase of the porosity compared to the heated samples. A similar behaviour has been also observed in the limestone samples. The open porosity obtained a higher increase in reference samples compared to the heated stones. This could be attributed to a higher pressure against the pore walls in the pores caused by crystallisation cycles [109], which has been more noticeable in the limestone due to the finer pore structure.

In the treated samples, both stones experimented an increase of open porosity after the salt crystallization cycles comparatively to the samples before the cycles. In the case of the granite, the open porosity yielded a similar increase in both treatments (18% for NE and 22% for NR). In the case of the limestone, samples treated with NE yielded a slightly higher increase compared to the limestone samples (29% for NE and 11% for NR). This is attributed to the lower presence of NR product on this stone. Additionally, the higher increase in porosity could be attributed to the difficulty of bonding a silicate material to calcite [12,110,111]. Wheeler also pointed out that the strength for limestone after ethyl silicate treatment is not that great as for sandstone [18]. Furthermore, other authors reported that, in calcareous stones with fine pores, silanes can fill the voids between calcite grains which can block the pores experiencing granular disintegration [112].

Stereomicroscopy allowed the identification of salt crystallization on the surfaces (Fig. 12). It was detected that those surfaces coated with NE, mainly limestone (Fig. 12C and G), showed a significant amount of salt acicular crystals.

FTIR spectra of the surfaces after 14 salt crystallization cycles are shown in Fig. 6. The thenardite crystals on the surfaces could be identified through the characteristic FTIR reflectance bands in the ranges corresponding to the vibrations of the SO_4^{2-} group and the Na–O vibrations; the most intense bands due to stretching of S–O bond is situated at 1100 cm^{-1} [113,114]. Therefore, on the

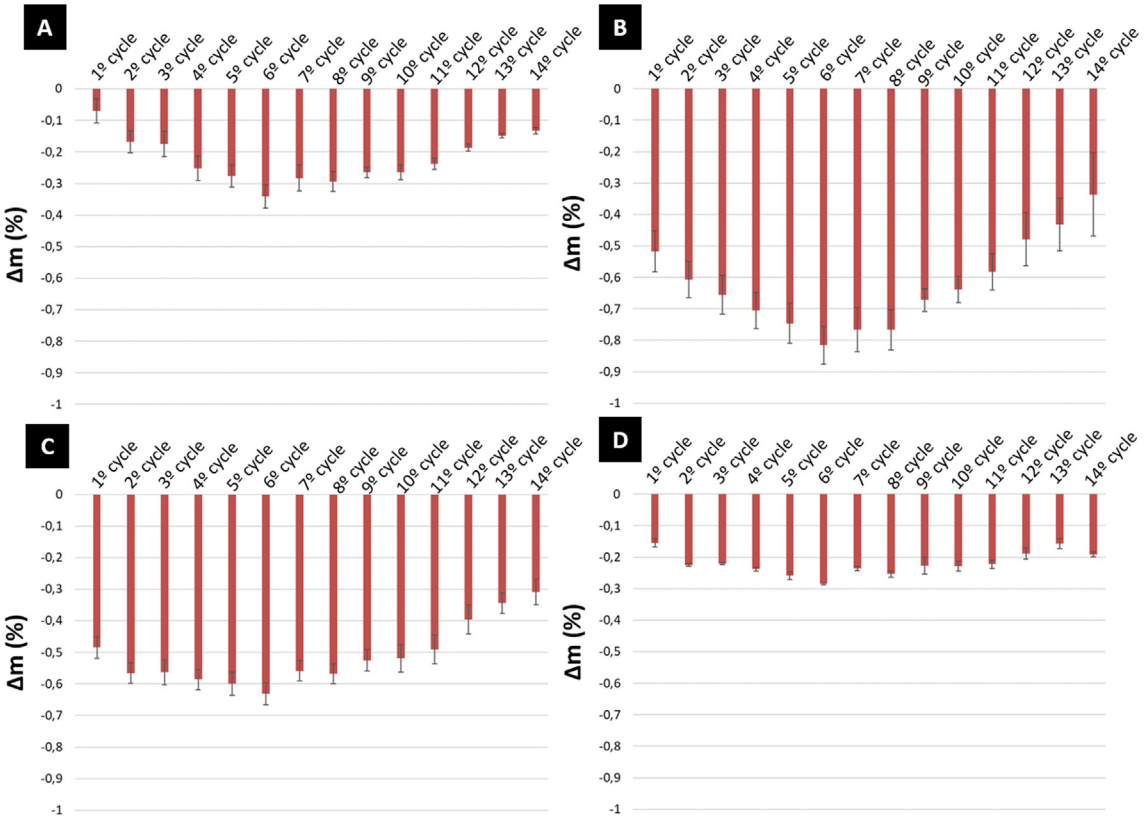

Fig. 10. Mass loss (Δm, %) in comparison with the original mass after each salt crystallization cycle for the granite samples. A: reference samples without nano-consolidant. B: samples exposed to 500 °C and cooled down with tap water immersion. C: samples exposed to 500 °C and consolidated with NE. D: samples exposed to 500 °C and consolidated with NR. Standard deviations are also shown. n = 5. NE: Nano Estel® and NR: Nanorestore®.

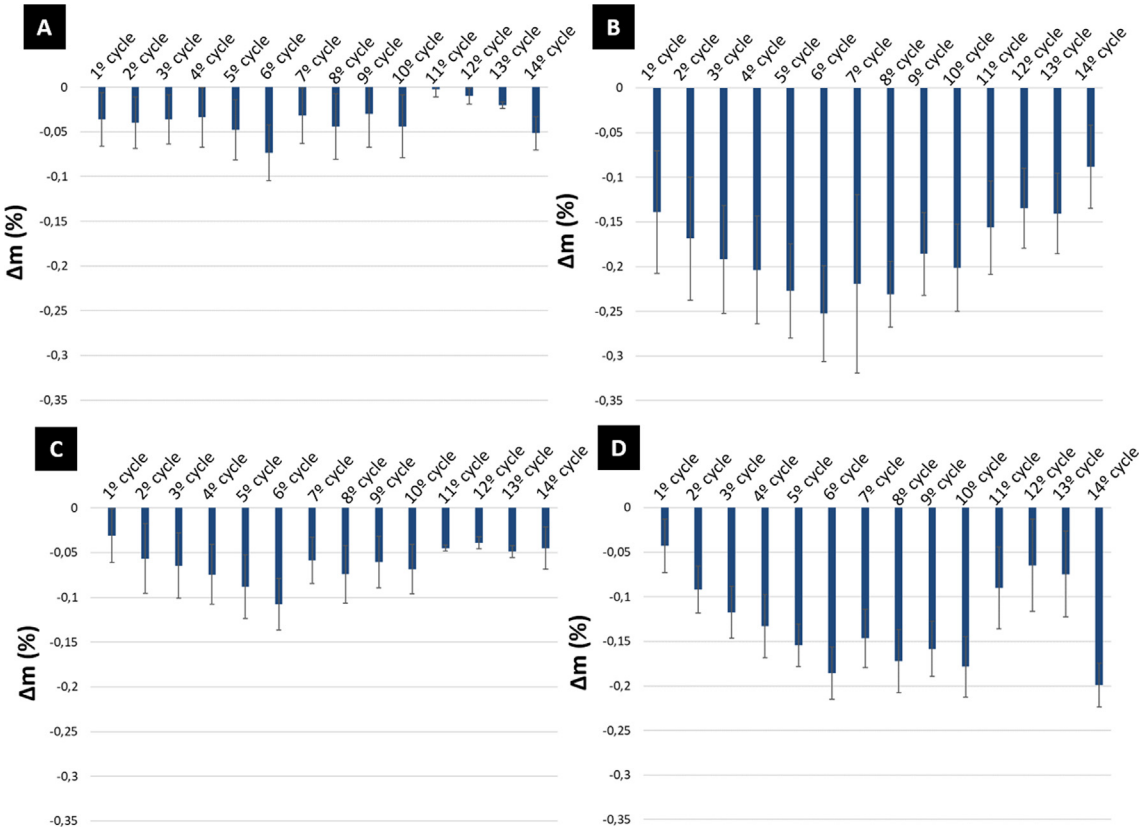

Fig. 11. Mass loss (Δm, %) in comparison with the original mass after each salt crystallization cycle for the limestone samples. A: reference samples without nano-consolidant. B: samples exposed to 500 °C and cooled down with tap water immersion. C: samples exposed to 500 °C and consolidated with NE. D: samples exposed to 500 °C and consolidated with NR. Standard deviations are also shown. n = 5. NE: Nano Estel® and NR: Nanorestore®.

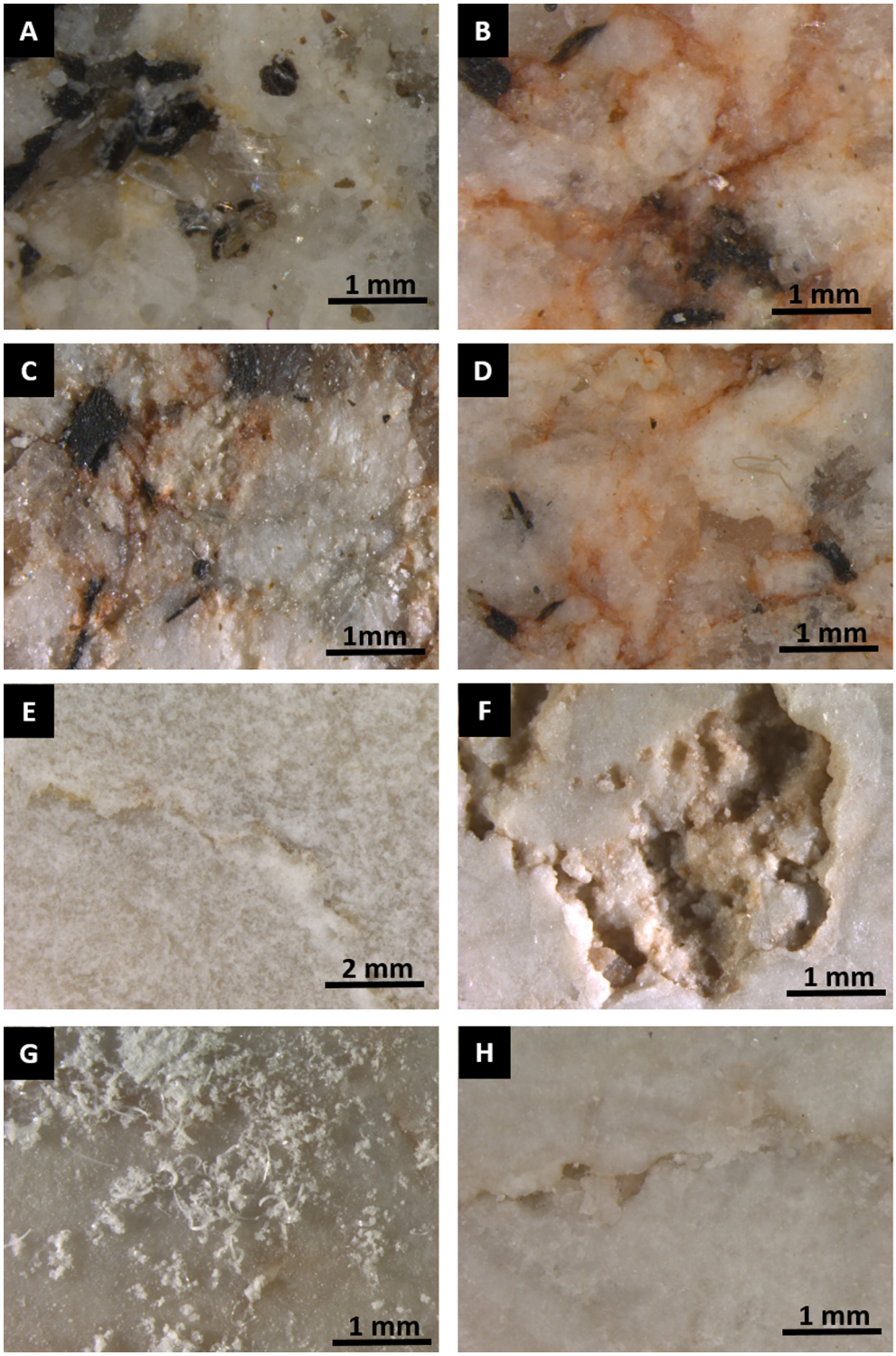

Fig. 12. Stereomicrographs of the granite (A-D) and limestone (E-H) samples after been exposed to fourteen salt crystallization cycles. A and E: reference samples without nano-consolidant. B and F: samples exposed to 500 °C and cooled down with tap water immersion. C and G: samples exposed to 500 °C and consolidated with NE. D and H: samples exposed to 500 °C and consolidated with NR. NE: Nano Estel® and NR: Nanorestore®.

evaluated surfaces, thenardite crystals were identified through a low band at 1100 cm^{-1} on the FTIR spectra of the surfaces of both stones coated with NR.

Visualization with SEM-EDS of the treated surfaces after the salt crystallization (Fig. 13) allowed the identification of crystals rich in sodium sulphate (thenardite). Conversely to La Russa et al. [40] working with Syton X30® (a suspension of nano-sized silica in water) and Estel 1000® (tetraethyl orthosilicate diluted in white spirit) on a tuff (a pyroclastic rock), columnar calcium sulphate (gypsum) grains were not detected in the limestone, despite this stone is a source of releasable calcium. SEM micrographs allowed to find that after the fourteen salt crystallization cycles, NE treatment was more cracked and less extensive throughout the progression of the crystallization cycles (Fig. 13A, E and F). On the surfaces covered with NR, it was observed that for the granite, the consolidant layer showed a lesser extent than the surface before

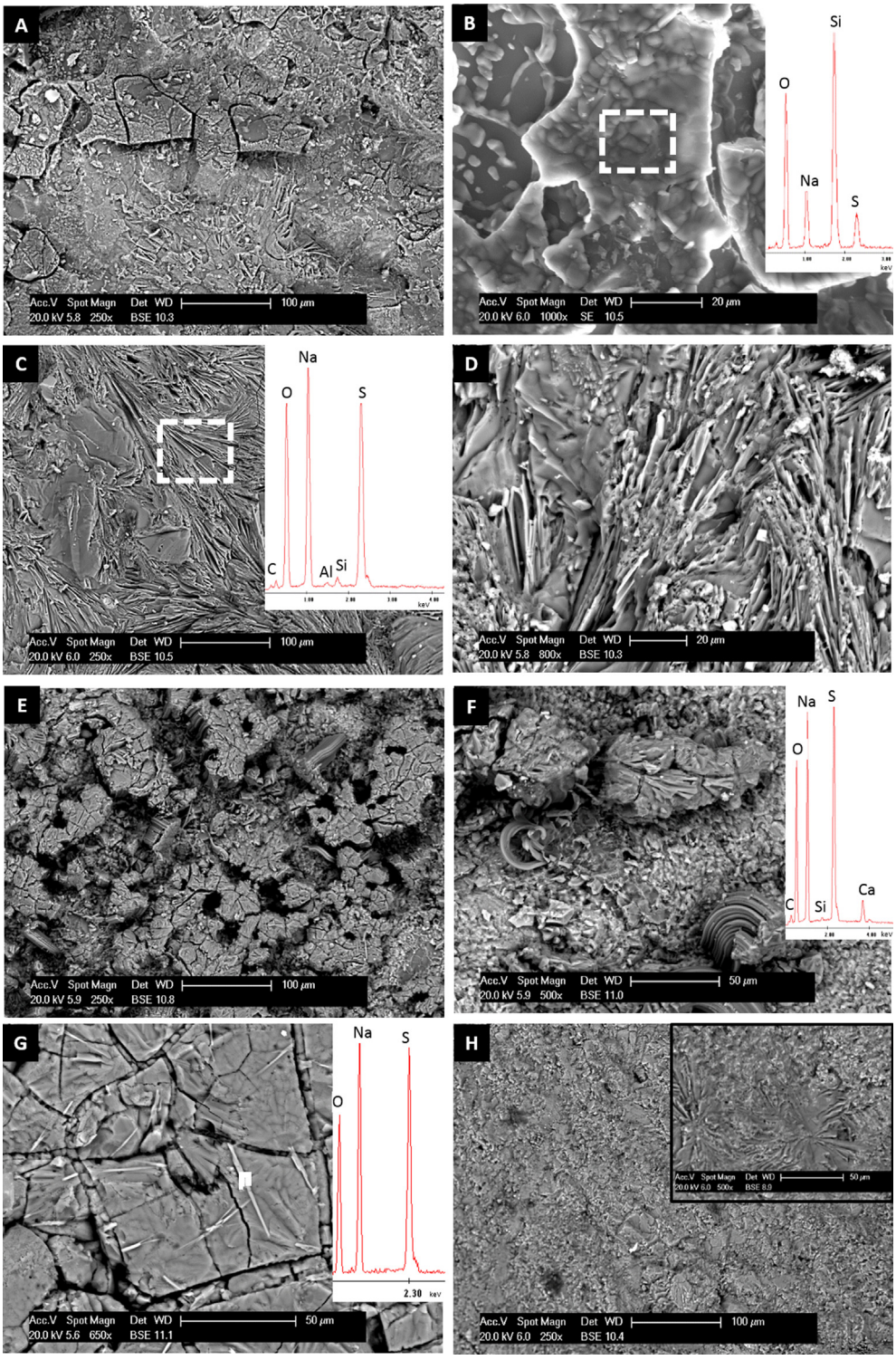

Fig. 13. SEM micrographs of the granite (A-D) and limestone (E-H) surfaces after fourteen salt crystallization cycles. Some of the micrographs are accompanied with the EDS spectrum of the area highlighted with a rectangle. A, B, E and G: surfaces exposed to 500 °C and consolidated with NE. C, D and H: surfaces exposed to 500 °C and consolidated with NR. NE: Nano Estel® and NR: Nanorestore®.

the crystallization cycles. On the surface of limestone covered with NR, the surface did not show a dense layer of consolidant previously to the application.

The thenardite after salt crystallization cycles showed different habitus considering the stone and the nanoconsolidant applied:

i) For granite coated with NE, clusters of tabular and pyramidal crystals rich is Na and S on the consolidant plates were found (Fig. 13A, B).
ii) For granite coated with NR, the entire surface of the sample was covered with well-formed planes rich in Na and S (Fig. 13C and D).

iii) For limestone coated with NE, deposits composed of acicular crystals (Fig. 13D and F) and single acicular crystals (Fig. 13G) rich in Na and S were found.
iv) For limestone coated with NR, it was barely found neo-formed deposits on the surface as the early stages of Na_2SO_4 planes, also found on the granite coated with NR (Fig. 12 H; see the detailed micrograph).

4. Conclusions

In this study, two different commercial nanoconsolidants (Nano Estel® and Nanorestore®) were evaluated in terms of consolidation effectiveness and durability. They were applied on two stones with different mineralogy and texture (a granite and a limestone), which are commonly used in the Cultural Heritage built in NW Iberian Peninsula. Both stones were previously weathered to obtain a loss of cohesion and increase the open porosity. Samples were subjected to 500 °C and rapidly cooled by tap water jet, simulating the effect caused by firefighters' intervention in a fire.

The results of this research have shown:

- After 500 °C, granite showed the highest increase of open porosity, which is associated to the fissures occurred after the heating and cooling down.
- Regarding the method used to applied both nanoconsolidants, different number of applications were used following Karsten pipe method; regardless of the product, higher number of applications were made in the granite and subsequently, higher dry matter was obtained.
- Nano Estel® and Nanorestore® induced different results due to their composition and the mineralogy of the stone. In the case of granite, similar reduction of the porosity and similar resistance to salt crystallization cycles were achieved. However, in the limestone, Nanorestore®, despite having a composition similar to the stone mineralogy, yielded lower effectiveness in terms of dry matter, porosity and water absorption by capillary coefficient, comparatively to the nanosilica consolidant. The lack of effectiveness was attributed to the low penetration of nanolime particles in the fine pore structure of this stone. However, the nanosilica consolidant Nano Estel® on the limestone induced higher levels of decay after crystallization cycles due to the difficulty to bond silicate materials to fine porous calcite-based substrates.
- Regarding the influence of the consolidant in the colour of the surfaces, granite yielded the highest surface colour alterations on samples treated with Nano Estel® due to the appearance of yellow spots.

One final conclusion of this study is that the effectiveness of both nanoconsolidants still needs to be fully understood when are applied to weathered substrates. This study provides more information about the behaviour of both products on two different stones. The results of this research could be key to determine the selection of a consolidant product in order to strengthen weathered substrates, especially those ones affected by fire and after the firefighters' intervention. Further works will be focused on the achievement of long term performance in terms of mechanical and physical properties and also on the influence of different environmental conditions on both nanoconsolidants.

Conflict of interest

None.

Acknowledgements

J.S. Pozo-Antonio was supported by the Ministry of Economy and Competitiveness, Government of Spain through grant number IJCI-2017-32771.

References

[1] ICOMOS, Ilustrated Glossary on Stone Deterioration Patterns. Monuments and Sites XVICOMOS-ICS, 2008.
[2] B. Chakrabarti, T. Yates, A. Lewry, Effect of fire damage on natural stonework in buildings, Constr. Build. Mater. 10 (7) (1996) 539–544, https://doi.org/10.1016/0950-0618(95)00076-3.
[3] R.J. Allison, G.E. Bristow, The effects of fire on rock weathering: some further considerations of laboratory experimental simulation, Earth Surf. Process. Landforms 24 (1999) 707–713.
[4] M.Y. Koca, G. Ozden, A.B. Yavuz, C. Kincal, T. Onargan, K. Kucuk, Changes in the engineering properties of marble in fire-exposed columns, Int. J. Rock Mech. Min. Sci. 43 (4) (2006) 520–530, https://doi.org/10.1016/j.ijrmms.2005.09.007.
[5] V. Pires, L.G. Rosa, A. Dionísio, Implications of exposure to high temperatures for stone cladding requirements of three Portuguese granites regarding the use of dowel–hole anchoring systems, Constr. Build. Mater. 64 (2014) 440–450, https://doi.org/10.1016/j.conbuildmat.2014.03.035.
[6] M. Hajpál, Á. Török, Mineralogical and colour changes of quartz sandstones by heat, Environ. Geol. 46 (3–4) (2004) 311–322, https://doi.org/10.1007/s00254-004-1034-z.
[7] E.M. Winkler, Stone in Architecture – Properties, Durability, Springer-Verlag, Berlin, 1997.
[8] V. Pires, P.M. Amaral, L.G. Rosa, R.S. Camposinhos, Slate flexural and anchorage strength considerations in cladding design, Constr. Build. Mater. 25 (10) (2011) 3966–3971, https://doi.org/10.1016/j.conbuildmat.2011.04.029.
[9] R. Esbert, J. Ordaz, F.J. Alonso, M. Montoto, Manual de Diagnosis y Tratamiento de Materiales Pétreos y Cerámicos, Collegi d'Aparelladors i Arquitectes Tècnics de Barcelona, Barcelona, 1997. ISBN: 84-87104-29-0, first ed..
[10] C. Cardell, T. Rivas, M.J. Mosquera, B. Prieto, J.M. Birginie, B. Silva, A. Moropoulou, R. Van Grieken, Patterns of damage in igneous and sedimentary rocks under conditions simulating sea-salt weathering, Earth Surf. Process Landforms 28 (2003) 1–14, https://doi.org/10.1002/esp.408.
[11] J. Ganor, E. Roueff, Y. Erel, J.D. Blum, The dissolution kinetics of a granite and its minerals—implications for comparison between laboratory and field dissolution rates, Geochim. Cosmochim. Acta 69 (3) (2005) 607–621, https://doi.org/10.1016/j.gca.2004.08.006.
[12] G. Wheeler, Alkoxysilanes and the consolidation of stone: where we are now, in: J. Delgado-Rodriguez, J.M. Mimoso (Eds.), Stone Consolidation in Cultural Heritage: Research and Practice, Proceedings of the International Symposium, LNEC (Laboratorio National de Engeneria Civil), Lisbon, Portugal, 2008, pp. 41–52.
[13] J. Otero, A.E. Charola, C.A. Grissom, V. Starinieri, An overview of nanolime as a consolidation method for calcareous substrates, Ge-conservación 11 (2017) 71–78.
[14] M. Favaro, R. Mendichi, F. Ossola, U. Russo, S. Simon, P. Tommasin, P.A. Vigato, Evaluation of polymers for conservation treatments of outdoor exposed stone monuments. Part I: photooxidative weathering, Polym. Degrad. Stab. 91 (2006) 3083–3096, https://doi.org/10.1016/j.polymdegradstab.2006.12.008.
[15] J.A. Schwarz, C. Contescu, A. Contescu, Methods for preparation of catalytic materials, Chem. Rev. 95 (1995) 477–510.
[16] E. Elaloui, A.C. Pierre, G.M. Pajonk, Influence of the sol-gel processing method on the structures and porous texture of non doped aluminas, J. Catal. 166 (1997) 340–347, https://doi.org/10.1006/jcat.1997.1540.
[17] F. Piacenti, R.G. Carbonell, M. Camaiti, F.E. Henon, E. Puppichini, Protective materials for stone-effects on stone permeability and gas transport, in: ICCROM (Ed.), Methods of Evaluating Products for the Conservation of Porous Building Materials in Monuments, 1995, pp. 389–402. Rome.
[18] F. Rubio, J. Rubio, J.L. Oteo, A FT-IR study of the hydrolysis of tetraethylorthosilicate TEOS, Spectrosc. Lett. 31 (1998) 199–219, https://doi.org/10.1080/00387019808006772.
[19] J. Brus, P. Kotlík, Cracking of organosilicon stone consolidants in gel form, Stud. Conserv. 41 (1996) 55–59, https://doi.org/10.2307/1506552.
[20] M.J. Mosquera, D.M. de los Santos, L. Valdez-Castro, L. Esquivias, New route for producing crack-free xerogels: obtaining uniform pore size, J. Non-Cryst. Solids 354 (2-9) (2008) 645–650, https://doi.org/10.1016/j.jnoncrysol.2007.07.095.
[21] J. Ashurst, The cleaning and treatment of limestone by the lime method, in: Conservation of Building and Decorative Stone, ed. J. Ashurst and F.G. Dimes, vol. 2 (1998), pp. 169–177. Butterworth-Heinemann Series in Conservation and Museology, London and Boston.
[22] I. Brajer, N. Kalsbeek, Limewater absorption and calcite crystal formation on a limewater-impregnated secco wallpainting, IIC Stud. Conserv. 44 (3) (1999) 145–156, https://doi.org/10.1179/sic.1999.44.3.145.
[23] P. Baglioni, D. Chelazzi, R. Giorgi, G. Poggi, Colloid and materials science for the conservation of cultural heritage: cleaning, consolidation, and deacidification, Langmuir 29 (2013) 5110–5122, https://doi.org/10.1021/la304456n.

[24] C. Price, K. Ross, G. White, A further appraisal of the 'lime technique' for limestone consolidation, using a radioactive tracer, Stud. Conserv. 33 (4) (1988) 178–186, https://doi.org/10.2307/1506313.
[25] J. Musacchi, T. Diaz Gonçalves, Influence of Nano-lime and Nano-silica Consolidants in the Drying Kinetics of Three Porous Building Materials, Internal Report 168, Laboratório Nacional de Engenharia Civil-LNEC, Lisbon, Portugal, 2014.
[26] S.A. Ruffolo, M.F. La Russa, M. Malagodi, C. Oliviero Rossi, A.M. Palermo, G.M. Crisci, ZnO and $ZnTiO_3$ nanopowders for antimicrobial stone coating, Appl. Phys. A 100 (2010) 829–834, https://doi.org/10.1007/s00339-010-5658-4.
[27] S.A. Ruffolo, M.F. La Russa, P. Aloise, C.M. Belfiore, A. Macchia, A. Pezzino, G.M. Crisci, Efficacy of nanolime in restoration procedures of salt weathered limestone rock, Appl. Phys. A 114 (2014) 753–758, https://doi.org/10.1007/s00339-013-7982-y.
[28] M.F. La Russa, S.A. Ruffolo, N. Rovella, C.M. Belfiore, A.M. Palermo, M.T. Guzzi, G.M. Crisci, Multifunctional TiO_2 coatings for cultural heritage, Prog. Org. Coat. 74 (2012) 186–191, https://doi.org/10.1016/j.porgcoat.2011.12.008.
[29] M.F. La Russa, A. Macchia, S.A. Ruffolo, F. De Leo, M. Barberio, P. Barone, G.M. Crisci, C. Urcí, Testing the antibacterial activity of doped TiO_2 for preventing biodeterioration of cultural heritage building materials, Int. Biodeter. Biodegr. 96 (2014) 87–96, https://doi.org/10.1016/j.ibiod.2014.10.002.
[30] P. Baglioni, D. Chelazzi, R. Giorgi, E. Carretti, N. Toccafondi, Y. Jaidar, Commercial $Ca(OH)_2$ nanoparticles for the consolidation of immovable works of art, Appl. Phys. A 114 (2014) 723–732, https://doi.org/10.1007/s00339-013-7942-6. DOI 10.1007/s00339-013-7942-6.
[31] C. Rodriguez-Navarro, E. Ruiz-Agudo, Nanolimes: from synthesis to application, Pure Appl. Chem. 90 (2017) 523–550, https://doi.org/10.1515/pac-2017-0506.
[32] M. Ambrosi, L. Dei, R. Giorgi, C. Neto, P. Baglioni, Colloidal particles of Ca $(OH)_2$, properties and applications to restoration of frescoes, Lagmuir 17 (14) (2001) 4251–4255, https://doi.org/10.1021/la010269b.
[33] G. Taglieri, J. Otero, V. Daniele, G. Gioia, L. Macera, V. Starinieri, A.E. Charola, The biocalcarenite stone of Agrigento (Italy): preliminary investigations of compatible nanolime treatments, J. Cultural Heritage 30 (2018) 92–99, https://doi.org/10.1016/j.culher.2017.11.003.
[34] V. Daniele, G. Taglieri, L. Macera, G. Rosatelli, J. Otero, A.E. Charola, Green approach for an eco-compatible consolidation of the Agrigento biocalcarenite surface, J. Constr. Build. Mater. 186 (2018) 1188–1199, https://doi.org/10.1016/j.conbuildmat.2018.08.033.
[35] S. Sequeira, C. Casanova, E.J. Cabrita, Deacidification of paper using dispersions of Ca(OH)2 nanoparticles in isopropanol, J. Cultural Heritage 7 (2006) 264–272, https://doi.org/10.1016/j.culher.2006.04.004.
[36] R. Giorgi, L. Dei, M. Ceccato, C. Schettino, P. Baglioni, Nanotechnologies for conservation of cultural heritage: paper and canvas deacidification, Langmuir 18 (21) (2002) 8198–8203, https://doi.org/10.1021/la025964d.
[37] I. Natali, P. Tempesti, E. Carretti, M. Potenza, S. Sansori, P. Baglioni, L. Dei 2, Aragonite crystals grown on bones by reaction of CO2 with nanostructured Ca (OH)2 in the presence of collagen. Implications in archaeology and paleontology, Langmuir 30 (2) (2014) 660–668.
[38] G. Poggi, N. Toccafondi, D. Chelazzi, P. Canton, R. Giorgi, P. Baglioni, Calcium hydroxide nanoparticles from solvothermal reaction for the deacidification of degraded waterlogged wood, J. Colloid Interface Sci. 473 (2016) 1–8.
[39] M.F. La Russa, S.A. Ruffolo, N. Rovella, C.M. Belfiore, P. Pogliani, C. Pelosi, M. Andaloro, G.M. Crisci, Cappadocian ignimbrite cave churches: stone degradation and conservation strategies, Period. Mineral. 83 (2) (2014) 187–206, https://doi.org/10.2451/2014PM0011.
[40] M.F. La Russa, S.A. Ruffolo, M.A. de Buergo, M. Ricca, C.M. Belfiore, A. Pezzino, G.M. Crisci, The behaviour of consolidated Neapolitan yellow Tuff against salt weathering, Bull. Eng. Geol. Environ. 76 (2017) 115–124, https://doi.org/10.1007/s10064-016-0874-6.
[41] G. Borsoi, M. Tavares, R. Veiga, A.S. Silva, Microstructural characterization of consolidant products for historical renders: an innovative nanostructured lime dispersion and a more traditional ethyl silicate limewater solution, Microsc. Microanal. 18 (5) (2012) 1181–1189, https://doi.org/10.1017/S1431927612001341.
[42] G. Borsoi, B. Lubelli, R. Van Hees, R. Veiga, A.S. Silva, Understanding the transport of nanolime consolidants within Maastricht limestone, J. Cult. Herit. 18 (2016) 1–8, https://doi.org/10.1016/j.culher.2015.07.014.
[43] A. Daehne, C. Herms, Calcium hydroxide nanosols for the consolidation of porous building materials, Heritage Sci. 1 (1) (2013) 1–11, https://doi.org/10.1186/2050-7445-1-11.
[44] J. Otero, V. Starinieri, A.E. Charola, Nanolime for the consolidation of lime mortars: a comparison of three available products, Constr. Build. Mater. 181 (2018) 394–407, https://doi.org/10.1016/j.conbuildmat.2018.06.055.
[45] E. Martinho, M. Mendes, A. Dionísio, 3D imaging of P-waves velocity as a tool for evaluation of heat induced limestone decay, Constr. Build. Mater. 135 (2017) 119–128, https://doi.org/10.1016/j.conbuildmat.2016.12.192.
[46] A. Zornoza-Indart, P. López-Arce, N. Leal, J. Simao, K. Zoghlami, Consolidation of a Tunisian bioclastic calcarenite: from conventional ethyl silicate products to nanostructured and nanoparticle based consolidants, Constr. Build. Mater. 116 (30) (2016) 188–202, https://doi.org/10.1016/j.conbuildmat.2016.04.114.
[47] IGME (Instituto Geológico y Minero de España), Mapa geológico de España. Serie Magna, E1:50.000, second ed., sheet 223-Vigo, 1985.
[48] J.S. Pozo-Antonio, A. Ramil, T. Rivas, A.J. López, M.P. Fiorucci, Effectiveness of chemical, mechanical and laser cleaning methods of sulphated black crusts developed on granite, Constr. Build. Mater. 112 (2016) 682–690, https://doi.org/10.1016/j.conbuildmat.2016.02.195.
[49] RILEM Recommandations provisoires, Essais recommandés pour mesurer l'altération des pièrres, Test n. II.1 Open Porosity, Commission 25 PEM, Protection et Erosion des Monuments, 1980.
[50] Z.C.G. Silva, Lioz—a royal stone in Portugal and a monumental stone in colonial Brazil, Geoheritage (2017), https://doi.org/10.1007/s12371-017-0267-7.
[51] I. de Rosario, F. Elhaddad, A. Pan, R. Benavides, T. Rivas, M.J. Mosquera, Effectiveness of a novel consolidant on granite: laboratory and in situ result, Constr. Build. Mater. 76 (2015) 140–149, https://doi.org/10.1016/j.conbuildmat.2014.11.055.
[52] M. Licchelli, M. Malagodi, M. Weththimuni, C. Zanchi, Nanoparticles for conservation of bio-calcarenite stone, Appl. Phys. A 114 (2014) 673–683, https://doi.org/10.1007/s00339-013-7973-z.
[53] B. Salvadori, L. Dei, Synthesis of $Ca(OH)_2$ nanoparticles from diols, Langmuir 17 (8) (2001) 2371–2374, https://doi.org/10.1021/la0015967.
[54] RILEM-Réunion Internationale des Laboratoires D'Essais et de Recherches sur les Matériaux et les Constructions, Recommandations provisoires de la commission 25-PEM Protection et érosion des monuments. Essais recommandes pour mesurer l'altération des pierres et évaluer l'efficacité des méthodes de traitement, in: Matériaux de Constructions, vol. 13, No. 75, RILEM, Paris, 1980.
[55] UNE-EN 1936:2006. Natural Stone Test Methods – Determination of Real Density and Apparent Density, and of Total and Open Porosity.
[56] UNE-EN 15801:2009. Conservation of Cultural Property – Test Methods – Determination of Water Absorption by Capillarity.
[57] UNE-EN 13755:2005, Natural stone test methods – Determination of water absorption at atmospheric pressure.
[58] CIE Publication 15-2, Colorimetry CIE Central Bureau, Vienna, 1986.
[59] CIE S014-4/E:2007Colorimetry Part 4: CIE 1976 L*a*b* Colour Space, Commission Internationale de l'eclairage, CIE Central Bureau, Vienna, 2007.
[60] B. Prieto, P. Sanmartín, B. Silva, F.M.M. Verdú, Measuring the color of granite rocks: a proposed procedure, Color Res. Appl. 35 (5) (2010) 368–375, https://doi.org/10.1002/col.20579.
[61] P. Sanmartín, P. Ferrer, V. Cárdenes, F. Martínez-Verdú, B. Silva, B. Prieto, El color de las rocas ornamentales: comparación de las metodologías de determinación en granitos y pizarras (The colour of ornamental rocks: comparison of determination methodologies in granites and slates)., in: IX Congreso Nacional del Color: Alicante, 29- 30 June, 1-2 July 2010. San Vicente del Raspeig: Publicaciones de la Universidad de Alicante, (2010) 433–436. ISBN 978-84- 9717-144-1.
[62] T. Rivas, J.M. Matías, J. Taboada, C. Ordóñez, Functional experiment design for the analysis of colour changes in granite using new L*a*b* functional colour coordinates, J. Comput. Appl. Math. 235 (16) (2011) 4701–4716, https://doi.org/10.1016/j.cam.2010.08.005.
[63] UNE-EN 12370: 1999, Natural Stone Test Methods – Determination of Resistance to Salt Crystallization.
[64] B Silva, T Rivas, B Prieto, Evaluation of the efficacy of the treatment of granitic rocks with two silicic consolidants, in: Moropoulou A, Zezza F, Kollias E, Papachristodooulou I, ed., Proc 4th International symposium on the conservation of monuments in the Mediterranean basin, Rhodes, May, 1997, vol. III. p. 375–384.
[65] T. Rivas, B. Prieto, B. Silva, Artificial weathering tests of granitic rocks, Mater. Construc. 58 (2008) 179–189, https://doi.org/10.3989/mc.2008.v58.i289-290.80.
[66] A.Z. Miller, N. Leal, L. Laiz, M.A. Rogerio-Candelera, R.J.C. Silva, A. Dionisio, M. F. Macedo, C. Saiz-Jiménez, Primary bio-receptivity of limestones used in Southern Europe monuments, in: B.J. Smith, M. Gómez-Heras, H.A. Viles, J. Cassar (Eds.), Limestone in the Built Environment: Present Day Challenges for the Preservation of the Past, Geological Society Special Publications, London, 2010, pp. 79–89. vol. 331.
[67] R. Capdevila and P. Floor. Les différents types de granites hercyniens et leur distribution dans le nord ouest de l'Espagne, Boletin Geoógico y Minero. T. LXXXI.-II-III (1970) 215–225.
[68] P. Vázquez, M. Acuña, D. Benavente, S. Gibeaux, I. Navarro, M. Gomez-Heras, Evolution of surface properties of ornamental granitoids exposed to high temperatures, Constr. Build. Mater. 104 (2016) 263–275, https://doi.org/10.1016/j.conbuildmat.2015.12.051.
[69] P. Vázquez, V. Shushakova, M. Gómez-Heras, Influence of mineralogy on granite decay induced by temperature increase: experimental observations and stress simulation, Eng. Geol. 189 (2015) 58–67, https://doi.org/10.1016/j.enggeo.2015.01.026.
[70] Z. Kompaníková, M. Gomez-Heras, J. Michnová, T. Durmeková, J. Vlcko, Sandstone alterations triggered by fire-related temperatures, Environ. Earth Sci. 72 (7) (2014) 2569–2581, https://doi.org/10.1007/s12665-014-3164-2.
[71] M. Gómez-Heras, M. Hajpál, M. Álvarez de Buergo, A. Torok, R. Fort, M.J. Varas, Evolution of porosity in Hungarian building stones after simulated burning, in: Proceedings of Heritage Weathering and Conservation HWC, Taylor & Francis, 2006, pp. 513–519.
[72] H. Yavuz, S. Demirdag, S. Caran, Thermal effect on the physical properties of carbonate rocks, Int. J. Rock Mech. Min. 47 (2010) 94–103, https://doi.org/10.1016/j.ijrmms.2009.09.014.
[73] E. Franzoni, E. Sassoni, G.W. Schererb, S. Naidu, Artificial weathering of stone by heating, J. Cult. Herit. 145 (2013) e85–e93, https://doi.org/10.1016/j.culher.2012.11.026.

[74] A. Ozguven, Y. Ozcelik, Investigation of some property changes of natural building stones exposed to fire and high heat, Const. Build. Mater. 38 (2013) 813–821, https://doi.org/10.1016/j.conbuildmat.2012.09.072.
[75] A.E. Charola, S.A. Centeno, K. Normandin, The New York public library: protective treatment for sugaring marble, J. Archit. Conserv. 16 (2) (2010) 29–44, https://doi.org/10.1080/13556207.2010.10785068.
[76] B.J. Skinner, Thermal expansion, in: S.P. Clark (Ed.), Handbook of Physical Constants, Geol. Soc. Am. Mem. (1996) 75–96.
[77] A.M. Barberena-Fernandez, M.T. Blanco-Varela, P.M. Carmona-Quiroga, Use of nanosilica- or nanolime-additioned TEOS to consolidate cementitious materials in heritage structures: physical and mechanical properties of mortars, Cem. Concr. Comp. (2018), https://doi.org/10.1016/j.cemconcomp.2018.09.011. in press.
[78] A. Arizzi, L.S. Gomez-Villalba, P. Lopez-Arce, G. Cultrone, R. Fort, Lime mortar consolidation with nanostructured calcium hydroxide dispersions: the efficacy of different consolidating products for heritage conservation, Eur. J. Mineral. 27 (3) (2015) 311–323, https://doi.org/10.1127/ejm/2015/0027-2437.
[79] J. Otero, V. Starinieri, A.E. Charola, Influence of substrate pore structure and nanolime particle size on the effectiveness of nanolime treatments, Constr. Build. Mater. (2018) in-press.
[80] A.E. Charola, E. Wendler, An overview of the water-porous building materials interactions, Restor. Build. Monuments 21 (2–3) (2015) 55–63, https://doi.org/10.1515/rbm-2015-2006.
[81] E. Zendri, G. Biscontin, I. Nardini, S. Riato, Characterization and reactivity of silicatic consolidants, Constr. Build. Mater. 21 (5) (2007) 1098–1106, https://doi.org/10.1016/j.conbuildmat.2006.01.006.
[82] M.J. Mosquera, T. Rivas, B. Prieto, B. Silva, Capillary rise in granitic rocks: interpretation of kinetics on the basis of pore structure, J. Colloid Interface Sci. 222 (2000) 41–45, https://doi.org/10.1006/jcis.1999.6612.
[83] G.W. Scherer, G.S. Wheeler, Silicate consolidants for stone, Key Eng. Mater 39 (2009) 1–25, https://doi.org/10.4028/www.scientific.net/KEM.391.1.
[84] E. Franzoni, B. Piginoa, C. Pistolesi, Ethyl silicate for surface protection of concrete: performance in comparison with other inorganic surface treatments, Cem. Concr. Comp. 44 (2013) 69–76, https://doi.org/10.1016/j.cemconcomp.2013.05.008.
[85] J.A. Bogas, M.G. Gomes, A. Gomes, Compressive strength evaluation of structural lightweight concrete by non-destructive ultrasonic pulse velocity method, Ultrasonics 53 (2013) 962–972, https://doi.org/10.1016/j.ultras.2012.12.012.
[86] P. Vázquez, F.J. Alonso, R.M. Esbert, J. Ordaz, Ornamental granites: Relationships between p-waves velocity, water capillary absorption and the crack network, Constr. Build. Mater. 24 (2010) 2536–2541, https://doi.org/10.1016/j.conbuildmat.2010.06.002.
[87] J. Escuder, R. Carbonell, D. Martí, A. Pérez-Estaún, Interacción fluido-roca a lo largo de las superficies de fractura: efectos mineralógicos y texturales de las alteraciones observadas en el Plutón Granítico de Albalá, SO del Macizo Hercínico Ibérico (Fluid-rock interaction along the fracture surfaces: mineralogical and textural effects of the alterations observed in the Granitic Pluton of Albalá, SW of the Iberian Hercynian Massif), Boletín Geológico y Minero 112 (3) (2001) 59–78.
[88] M. Gómez-Heras, Procesos y formas de deterioro térmico en piedra natural del patrimonio arquitectónico (Processes and forms of thermal deterioration in natural stone of the architectural heritage) PhD Thesis, Universidad Complutense de Madrid, 2005.
[89] J.S. Pozo-Antonio, T. Rivas, F. Carrera, L. García, Deterioration processes affecting prehistoric rock art engravings in granite in NW Spain, Earth Surf. Process. Landf. 43 (2018) 2435–2448, https://doi.org/10.1002/esp.4406.
[90] A. Dionisio, M.A. Braga, J.C. Waerenborgh, Clay minerals and iron oxidesoxyhydroxides as fingerprints of firing effects in a limestone monument, Appl. Clay Sci. 42 (2009) 629–638, https://doi.org/10.1016/j.clay.2008.05.003.
[91] G. Borsoi, R. Veiga, A. Santos Silva, Effect of nanostructured lime-based and silica-based products on the consolidation of historical renders, 3rd Historic Mortars Conference, 11-14 September 2013, Glasgow, Scotland.
[92] J.F. Illescas, M. Mosquera, Surfactant-synthesized PDMS/silica nanomaterials improve robutness and stain resistance of carbonate stone, J. Phys. Chem. C 115 (30) (2011) 14624–14634, https://doi.org/10.1021/jp203524p.
[93] A. Pondelak, S. Kramar, M. Lesar Kikelj, A. Sever Skapin, In-situ study of the consolidation of wall paintings using commercial and newly developed consolidants, J. Cult. Herit. 28 (2017) 1–8, https://doi.org/10.1016/j.culher.2017.05.014.
[94] L. Dei, B. Salvadori, Nanotechnology in cultural heritage conservation: nanometric slaked lime saves architectonic and artistic surfaces from decay, J. Cult. Herit. 7 (2) (2006) 110–115, https://doi.org/10.1016/j.culher.2006.02.001.
[95] I. Natali, M.L. Saladino, F. Andriulo, D.C. Martino, E. Caponetti, E. Carretti, L. Dei, Consolidation and protection by nanolime: recent advances for the conservation of the graffiti, Carceri dello Steri Palermo and of the 18th century lunettes, SS. Giuda e Simone Cloister, Corniola (Empoli), J. Cult. Herit. 15 (2) (2014) 151–158, https://doi.org/10.1016/j.culher.2013.03.002.
[96] W.S. Mokrzycki, M. Tatol, Colour difference ΔE – a survey, Machine Graphics Vision 20 (4) (2011) 383–411.
[97] J. Delgado-Rodrigues, A. Grossi, Indicators and ratings for the compatibility assessment of conservation actions, J. Cult. Herit. 8 (1) (2007) 32–43, https://doi.org/10.1016/j.culher.2006.04.007.
[98] A.M. Barberena-Fernández, P.M. Carmona-Quiroga, M.T. Blanco-Varela, Interaction of TEOS with cementitious materials: chemical and physical effects, Cem. Concr. Comp. 55 (2015) 145–152, https://doi.org/10.1016/j.cemconcomp.2014.09.010.
[99] R. Liu, X. Han, X. Huang, W. Li, H. Luo, Preparation of three-component TEOS-based composites for stone conservation by sol–gel processes, J. Sol-Gel Sci. Technol. 68 (2013) 19–30, https://doi.org/10.1007/s10971-013-3129-z.
[100] R. Esbert, J. Alonso-Sánchez, Hidrofugación de rocas carbonatadas porosas: propiedades que controlan su eficacia (Water-repelling treatment of porous carbonate rocks: Properties that control their effectiveness), Mater. Construc. 45 (237) (1995) 15–30, https://doi.org/10.1007/s10971-013-3129-z.
[101] C. Rodriguez-Navarro, A. Suzuki, E. Ruiz-Agudo, Alcohol dispersions of calcium hydroxide nanoparticles for stone conservation, Langmuir 29 (2013) 11457–11470, https://doi.org/10.1021/la4017728.
[102] A.M. Berberena Fernández, Conservación de esculturas de hormigón: efecto de consolidantes en pastas y morteros de cemento (Conservation of concrete sculptures: effect of consolidants in cement pastes and mortars) PhD Thesis, Universidad Complutense de Madrid, 2016.
[103] S. Gopi, V.K. Subramanian, Anomalous transformation of calcite to vaterite: significance of HEDTA on crystallization behaviour and polymorphism at elevated temperatures, Indian J. Chem. 52A (3) (2013) 342–349. http://hdl.handle.net/123456789/16297.
[104] R.J. Gilkes, A. Suddhiprakarn, Biotite alteration in deeply weathered granite. I. morphological, mineralogical and chemical properties, Clays Clay Miner. 27 (5) (1979) 349–360.
[105] S. Gialanella, F. Girardi, G. Ischia, I. Lonardelli, M. Mattarelli, M. Montagna, On the goethite to hematite phase transformation, J. Therm. Anal Calorim 102 (2010) 867–873, https://doi.org/10.1007/s10973-010-0756-2.
[106] Y. Wen, L. Xiang, Y. Jin, Synthesis of plate-like calcium carbonate via carbonation route, Mater. Lett. 57 (2003) 2565–2571, https://doi.org/10.1016/S0167-577X(02)01312-5.
[107] J. Margret, J. Geselbracht, R. College, Sol-gel Silica: Nanoarquitectured of Being and Nothingness, VIPERr-virtual Inorganic Pedagogical electronic resource, IONiC – Interactive Online Network of Inorganic Chemists, 2009.
[108] P. López-Arce, L.S. Gómez-Villalba, S. Martínez-Ramírez, M. Álvarez de Buergo, R. Fort, Influence of relative humidity on the carbonation of calcium hydroxide nanoparticles and the formation of calcium carbonate polymorphs, Powder Technol. 205 (2011) 263–269, https://doi.org/10.1016/j.powtec.2010.09.026.
[109] A.E. Charola, Salts in the deterioration of porous materials: an overview, J. Am. Instit. Conserv. 39 (3) (2000) 327–343, https://doi.org/10.1179/019713600806113176.
[110] A.P. Ferreira Pinto, J. Delgado Rodrigues, Stone consolidation: the role of treatment procedures, J. Cult. Herit. 9 (1) (2008) 38–53, https://doi.org/10.1016/j.culher.2007.06.004.
[111] A.P. Ferreira-Pinto, J. Delgado-Rodrigues, Hydroxylating conversion treatment and alkoxysilane coupling agent as pre-treatment for the consolidation of limestones with ethyl silicate, in: J. Delgado-Rodriguez, J. M. Mimoso (Eds.), Stone Consolidation in Cultural Heritage: Research and Practice; Proceedings of the International Symposium, Lisbon, 6-7 May 2008, LNEC (Laboratorio National de Engenheria Civil), Lisbon, 2008, pp. 41–52.
[112] J. Ruedrich, T. Weiss, S. Siegesmund, Thermal behaviour of consolidated marbles, in: S. Siegesmund, T. Weiss, A. Vollbrecht (Eds.), Natural Stone, Weathering Phenomena, Conservation Strategies and Case Studies, The Geological Society of London, London, 2002, pp. 255–271. Geological Society Special Publication N°. 205.
[113] Y.S. Vidya, B.N. Lakshminarasappa, Preparation, characterization, and luminescence properties of orthorhombic sodium sulphate, Phys. Res. Int. (2013), https://doi.org/10.1155/2013/641631.
[114] I. Arrizabalaga, O. Gómez-Laserna, J.A. Carrero, J. Bustamante, A. Rodriguez, G. Arana, J.M. Madariaga, Diffuse reflectance FTIR database for the interpretation of the spectra obtained with a handheld device on built heritage materials, Anal. Methods 7 (2015) 1061–1070, https://doi.org/10.1039/c4ay02189d.